DEPARTMENT OF MATHEMATICS

The Application of Roe's Scheme to Two Problems of Engineering Interest.

by

A. Priestley

Numerical Analysis Report **8/92**

UNIVERSITY OF READING

Final Report on the Contract entitled "New Numerical Algorithms for Conservation Laws" for ENEL-CRIS, Milan, Italy.*

A. Priestley

Institute of Computational Fluid Dynamics,

Department of Mathematics,

University of Reading,

Whiteknights,

Reading,

United Kingdom.

August 25, 1992

*The work reported here forms part of the research programme of the Reading/Oxford Institute for Computational Fluid Dynamics and was funded by ENEL-CRIS Milan, Italy.

0 Abstract

The purpose of this report is to describe work carried out on the above contract concerning the feasibility of using Roe's scheme for problems of interest to ENEL. This scheme gives approximate solutions of processes governed by systems of hyperbolic conservation laws and applies to both problems of water flow, dam-breaks for example, and of gas flow. Although the Euler equations for gas flow have much in common with the shallow water equations the types of flow expected are quite different. High speed gas flows are dominated by discontinuous shocks and expansion waves. In shallow water flow, on the other hand, many interesting flows have 'smooth' solutions and classical methods will solve these accurately and efficiently. However, there are situations where discontinuities arise, the dam-break problem for one, and classical methods often struggle to give acceptable answers to these problems. Discontinuities are, therfore, an integral part of many problems involving systems of conservation laws and Roe's method has been specially developed for solving these problems.

In this work we have sought to show the potential of the method in areas of special interest to ENEL–CRIS. It is hoped that the work will show whether or not this new solution technique will provide an algorithm that is robust, and accurate, enough to provide a numerical method suitable for many of the flow problems arising at ENEL.

1 Introduction

In order to test the suitability of Roe's Total Variation Diminishing (TVD) scheme, see Roe [15, 16] for example, ENEL suggested two test problems for which there is test data that can be used to verify the codes. The first involves a dambreak situation and the second is that of a blast wave exiting from a muzzle. Both involve the solution of a hyperbolic system of non-linear equations, the shallow water equations or the Euler equations. In both cases the non-linear equations are decomposed, using an approximate Riemann solver, into a number of wave problems. Each of these wave, or advection, problems can then be evolved using a TVD scheme, see Sweby [19] for example. In this report we will be concerned only with the approximate Riemann solver due to Roe [15] and schemes that arise from this.

In the following section Roe's Scheme will be derived for the 1-D shallow water equations and then for the 2-D shallow water equations. A discussion will also be given as to applying these essentially 1-D scheme in more than one-dimension.Then in section 3 the test problems for the 2-D shallow water equations will be described and the results to this problem will be given.

In section 4 we will move on to the application of Roe's scheme to the 1-D and 2-D Euler equations, in particular those governing axially symmetric flows. A test problem for these equations will be described and the results given.

Finally we summarise this work in section 5.

2 Roe's Scheme for the Shallow Water Equations

2.1 One-Dimension

The usual form of the shallow water equations in one-dimension are given, for our purposes, by the St. Venant equations. These are

$$\frac{\partial A}{\partial t} + \frac{\partial Q}{\partial x} = 0 \tag{2.1}$$

$$\frac{\partial Q}{\partial t} + \frac{\partial}{\partial x}\left(\frac{Q^2}{A}\right) + gA\left[\frac{\partial h}{\partial x} + S_f\right] = 0, \tag{2.2}$$

where

A = cross-sectional area = breadth $\times$ depth = $B \times d$

(only rectangular channels are considered here)

u = velocity

Q =massflow

g =acceleration due to gravity

h =height= $d + z$where z is the height of the river bed

S_f is a friction term. A typical form of this is $\frac{Q|Q|}{K^2}$ where

$K = \frac{A}{M}$(hydraulic radius)$^{2/3}$ and M is Manning's constant.

Before proceeding we rewrite equation 2.2 in a conservation form

more suitable for the application of Roe's scheme, namely,

$$Q_t + \left(\frac{Q^2}{A} + \frac{gA^2}{2B}\right)_x = gA\left(\frac{AB_x}{2B^2} - S_f - \beta\right) \tag{2.3}$$

where we have replaced h by $A/B + z$ and $\beta = z_x$. The equations, (2.1) and (2.3), are now in the form we shall require and can be written in vector notation as

$$\underline{q}_t + \underline{F}_x = \underline{b}$$

where

$$\underline{q} = \begin{pmatrix} A \\ Q \end{pmatrix} \tag{2.4}$$

$$\underline{F} = \begin{pmatrix} Q \\ \frac{Q^2}{A} + \frac{1}{2}g\frac{A^2}{B} \end{pmatrix} \tag{2.5}$$

$$\underline{b} = \begin{pmatrix} 0 \\ gA\left(\frac{AB_x}{B^2} - S_f - \beta\right) \end{pmatrix}. \tag{2.6}$$

An extra $\frac{1}{2}gA^2B_x/B^2$ has been added to both sides of the equation for reasons which we shall give later. Following Roe [15] we define an intermediate, or parameter, vector

$$\underline{w} = \begin{pmatrix} w_1 \\ w_2 \end{pmatrix} = \begin{pmatrix} A^{\frac{1}{2}} \\ uA^{\frac{1}{2}} \end{pmatrix}. \tag{2.7}$$

(The definition of this vector is somewhat arbitrary and the scheme can be derived without its use, relying solely on the properties that the resulting differences and averages must have. The use of the parameter vector in the form given here

merely simplifies the derivation, by removing several layers of algebra.) The vectors $\underline{q}$ and $\underline{F}$, equations (2.4,2.5), can now be expressed in terms of the parameter vector variables, w_1, w_2, as

$$\underline{q} = \begin{pmatrix} w_1^2 \\ \\ w_1 w_2 \end{pmatrix}, \quad \underline{F} = \begin{pmatrix} w_1 w_2 \\ \\ w_2^2 + \frac{1}{2} g w_1^4 / B \end{pmatrix}.$$

Using the standard notation of $\Delta\underline{x} = \underline{x}_R - \underline{x}_L$ and $\overline{\underline{x}} = \frac{1}{2}(\underline{x}_R + \underline{x}_L)$ we proceed to calculate matrices $B(\underline{w})$ and $C(\underline{w})$ such that

$$\Delta\underline{q} = B(\underline{w})\Delta\underline{w} \tag{2.8}$$

$$\Delta\underline{F} = C(\underline{w})\Delta\underline{w}. \tag{2.9}$$

This leads to

$$B = \begin{pmatrix} 2\overline{w_1} & 0 \\ \\ \overline{w_2} & \overline{w_1} \end{pmatrix}$$

and

$$C = \begin{pmatrix} \overline{w_2} & \overline{w_1} \\ \\ \frac{2g}{B^{*2}} \overline{B}\, \overline{w_1^2}\, \overline{w_1} & 2\overline{w_2} \end{pmatrix},$$

where $B^* = \sqrt{B_L B_R}$.

At least this is what we would like to have done. Unfortunately not all the terms can be expressed in this fashion — essentially jumps in $\underline{F}$ due to changes in B cannot be accounted for in terms of jumps in $\underline{w}$ — and so an

extra $\frac{1}{2}gA^2B_x/B^2$ must be added to both sides of equation (2.3).

To decompose the problem into its characteristic components we proceed to find λ such that

$$\det(\lambda B - C) = 0, \tag{2.10}$$

giving

$$\lambda_1 = \frac{\overline{w_2}}{\overline{w_1}} - \sqrt{g\overline{B}\,\overline{w_1^2}/B^{*2}}$$

$$\lambda_2 = \frac{\overline{w_2}}{\overline{w_1}} + \sqrt{g\overline{B}\,\overline{w_1^2}/B^{*2}}.$$

Reassuringly, if we ignore the averaging, these then simplify to $u \pm \sqrt{gd}$ as we would expect.

These eigenvalues give two eigenvectors which, after multiplication by the matrix B, are given by :-

$$\underline{e}_1 = \begin{pmatrix} \overline{w_1} \\ \overline{w_2} - \sqrt{g\overline{B}\,\overline{w_1^2}\,\overline{w_1}^2/B^{*2}} \end{pmatrix}$$

$$\underline{e}_2 = \begin{pmatrix} \overline{w_1} \\ \overline{w_2} + \sqrt{g\overline{B}\,\overline{w_1^2}\,\overline{w_1}^2/B^{*2}} \end{pmatrix}.$$

Two α's, representing wave-strengths, are now found such that $\sum_i \alpha_i \underline{e}_i = \Delta \underline{q}$ (and by construction $\sum_i \alpha_i \lambda_i \underline{e}_i = \Delta \underline{F}$), i.e.,

$$\alpha_1 = \Delta w_1 - \frac{\overline{w}_1 \Delta w_2 - \overline{w}_2 \Delta w_1}{2\sqrt{g\overline{B}\,\overline{w^2}_1\,\overline{w}_1^2/B^{*2}}}$$

$$\alpha_2 = \Delta w_1 + \frac{\overline{w}_1 \Delta w_2 - \overline{w}_2 \Delta w_1}{2\sqrt{g\overline{B}\,\overline{w^2}_1\,\overline{w}_1^2/B^{*2}}}$$

The flux difference, $\Delta \underline{F}$, caused by the jump in two neighbouring piecewise constant states, $\Delta \underline{q}$, has now been split into a number of wave problems where the $\underline{e}_j$'s can be regarded as the waves, the λ_j's as the wave speeds and the α_j's as the wave strengths. We can now apply standard TVD type algorithms to each of these wave problems as follows.

If we define $\phi_{j,i+\frac{1}{2}}$ to be the signal from the j^{th} eigenvalue at the jump at $i+\frac{1}{2}$, i.e.,

$$\phi_{j,i+\frac{1}{2}} = -\frac{\Delta t}{\Delta x}\lambda_j \alpha_j \underline{e}_j$$

then the first order upwind algorithm is defined by:-

$$\text{if} \quad \left\{ \begin{array}{l} \lambda_j > 0 \\ \\ \lambda_j < 0 \end{array} \right\} \quad \text{then add } \phi_{j,i+\frac{1}{2}} \text{ to} \quad \left\{ \begin{array}{l} \underline{q}_{i+1} \\ \\ \underline{q}_i \end{array} \right. .$$

If we, in addition, transfer an amount $a_{j,i+\frac{1}{2}}$ against the direction of flow we can achieve second order accuracy in smooth regions by choosing

$$a_j = \frac{1}{2}(1 - |\nu_j|)$$

where ν_j is the CFL number of the j^{th} wave.

Defining a transfer function, Baines [1], by

$$B(a_{j,i+\frac{1}{2}}\phi_{j,i+\frac{1}{2}}, a_{j,i+\frac{1}{2}-\sigma_j}\phi_{j,i+\frac{1}{2}-\sigma_j}) = B(b_1, b_2),$$

say, where $\sigma_j = sign(\lambda_j)$, we can arrive at various second order schemes. Linear functions of b_1 & b_2 tend to give classical second order schemes (for a scalar equation) with all their faults when approximating discontinuous solutions. For example, $B(b_1, b_2) = b_1$ is the Lax-Wendroff scheme, $B(b_1, b_2) = b_2$ is the second order fully upwind scheme and $B(b_1, b_2) = \frac{1}{2}(b_1 + b_2)$ is Fromm's algorithm. For non-linear systems these schemes will not be identical to their classical ancestors but they will tend to exhibit the same properties. Taking non-linear functions of b_1 & b_2, however, enables us to arrive at oscillation-free second order schemes (see Sweby [19, 20] for a fuller discussion).

Three of the most useful limiters are the minmod limiter, [19], Van Leer's limiter, see Van Leer [21], and the Superbee limiter, Roe [16]. With all these limiters they return a value of $B(b_1, b_2) = 0$ if $b_1 b_2 < 0$. In the case of the b's having the same sign we then have:-

$$\text{(2.11)} \qquad \text{Minmod} \quad B(b_1, b_2) = \begin{cases} b_1 & \text{if } |b_1| < |b_2| \\ b_2 & \text{if } |b_1| > |b_2| \end{cases}$$

$$\text{Van Leer's limiter} \quad B(b_1, b_2) = \frac{2b_1 b_2}{(b_1 + b_2)}$$

$$\text{Superbee} \qquad B(b_1, b_2) \;=\; \begin{cases} b_1 & 1 \le \frac{b_1}{b_2} \le 2 \\ b_2 & 1 \le \frac{b_2}{b_1} \le 2 \\ 2b_2 & \frac{b_1}{b_2} \ge 2 \\ 2b_1 & \frac{b_2}{b_1} \ge 2 \end{cases}.$$

We note, for future reference, that the source terms, $\underline{b}$, from equation (2.6), can be expanded in terms of the eigenvectors $\underline{e}_1$ & $\underline{e}_2$ as $\underline{b} = \beta_1 \underline{e}_1 + \beta_2 \underline{e}_2$ where

$$\beta_1 \;=\; \frac{-\sqrt{g}(AB_x/B^{*^2} - S_f - \beta)B^*}{2\sqrt{B}}$$

$$\beta_2 \;=\; -\beta_1.$$

2.2 Two-Dimensions

In two-dimensions the shallow water equations we shall be using can be written in the form

$$\underline{q}_t + \underline{F}_x + \underline{G}_y = \underline{b} \tag{2.12}$$

where

$$\underline{q} \;=\; \begin{pmatrix} h \\ hu \\ hv \end{pmatrix},$$

$$\underline{F} = \begin{pmatrix} hu \\ hu^2 + gh^2/2 \\ huv \end{pmatrix},$$

$$\underline{G} = \begin{pmatrix} hv \\ huv \\ hv^2 + gh^2/2 \end{pmatrix},$$

$$\underline{b} = \begin{pmatrix} 0 \\ gh(\beta_x - S_f^x) \\ gh(\beta_y - S_f^y) \end{pmatrix}.$$

β_x and β_y are just the bed-slopes in the x and y directions respectively,

$$\beta_x = -\frac{\partial z}{\partial x}, \quad \beta_y = -\frac{\partial z}{\partial y}.$$

The friction terms we shall be using in the computations here are defined in equation (2.13) as

$$S_f^x = \frac{n^2 u\sqrt{u^2+v^2}}{h^{4/3}}, \quad S_f^y = \frac{n^2 v\sqrt{u^2+v^2}}{h^{4/3}}. \tag{2.13}$$

In (2.13) Manning's constant is denoted by n and takes the value 0.012 for the dambreak problems of section 3. Instead of h, the height, we actually use the variable $\phi = gh$ and define the momenta to be $m = \phi u$ and $n = \phi v$. This is an inconsequential difference as far as the method is concerned and we could as easily proceed using h.

There is some concern about using essentially one-dimensional models for multi-dimensional problems and there has recently been some effort to

create genuinely multi-dimensional upwind codes, see Deconinck et al. [6], Hirsch & Lacor [10] and Roe [17] for example. However, these algorithms have been developed solely for the Euler equations at this point and are at a very early stage of development. Hence the vast majority of practitioners use the splitting approach. That is, we regard the problem

$$\underline{q}_t + \underline{F}_x + \underline{G}_y = 0$$

as two one-dimensional problems

$$\underline{q}_t + \underline{F}_x = 0$$

$$\underline{q}_t + \underline{G}_y = 0$$

to which the one-dimensional algorithm can now be applied, see Strang [18] for example.

Following the procedure explained for the one-dimensional case we define a parameter vector

$$\underline{w} = \begin{pmatrix} w_1 \\ w_2 \\ w_3 \end{pmatrix} = \begin{pmatrix} \phi^{\frac{1}{2}} \\ \phi^{\frac{1}{2}} u \\ \phi^{\frac{1}{2}} v \end{pmatrix}$$

and now express the vectors $\underline{q}, \underline{F}$ & $\underline{G}$ in terms of these variables to get

$$\underline{q} = \begin{pmatrix} w_1^2 \\ w_1 w_2 \\ w_1 w_3 \end{pmatrix}, \quad \underline{F} = \begin{pmatrix} w_1 w_2 \\ w_2^2 + \frac{w_1^4}{2} \\ w_2 w_3 \end{pmatrix}, \quad \underline{G} = \begin{pmatrix} w_1 w_3 \\ w_2 w_3 \\ w_3^2 + \frac{w_1^4}{2} \end{pmatrix}.$$

Considering just the x-direction we again look for matrices $B(\underline{w})$ and $C(\underline{w})$ as in equations (2.8) and (2.9). This now leads to

$$B = \begin{pmatrix} 2\overline{w}_1 & 0 & 0 \\ \overline{w}_2 & \overline{w}_1 & 0 \\ \overline{w}_3 & 0 & \overline{w}_1 \end{pmatrix},$$

$$C = \begin{pmatrix} \overline{w}_2 & \overline{w}_1 & 0 \\ 2\overline{w}_1\overline{w^2}_1 & 2\overline{w}_2 & 0 \\ 0 & \overline{w}_3 & \overline{w}_2 \end{pmatrix}.$$

As in (2.10) we calculate

$$\lambda^F_{1,2,3} = \frac{\overline{w}_2}{\overline{w}_1} - \sqrt{\overline{w^2}_1}, \quad \frac{\overline{w}_2}{\overline{w}_1}, \quad \frac{\overline{w}_2}{\overline{w}_1} + \sqrt{\overline{w^2}_1}$$

which are sen to be the $u, u \pm \sqrt{\phi}$ characteristic speeds we would have expected. These eigenvalues then lead to three eigenvectors which, after multiplication by the matrix B, are

$$\underline{e}^F_{1,2,3} = \left\{ \begin{pmatrix} \overline{w}_1 \\ \overline{w}_2 - \overline{w}_1\sqrt{\overline{w^2}_1} \\ \overline{w}_3 \end{pmatrix}, \begin{pmatrix} 0 \\ 0 \\ \overline{w}_1 \end{pmatrix}, \begin{pmatrix} \overline{w}_1 \\ \overline{w}_2 + \overline{w}_1\sqrt{\overline{w^2}_1} \\ \overline{w}_3 \end{pmatrix} \right\}.$$

The wave strengths can then be found as

$$\left\{ \begin{array}{c} \alpha_1^F \\ \alpha_2^F \\ \alpha_3^F \end{array} \right\} = \left\{ \begin{array}{c} \Delta w_1 - \frac{\overline{w}_1 \Delta w_2 - \overline{w}_2 \Delta w_1}{2\overline{w}_1 \sqrt{\overline{w^2}_1}} \\ \frac{\overline{w}_1 \Delta w_3 - \overline{w}_3 \Delta w_1}{\overline{w}_1} \\ \Delta w_1 + \frac{\overline{w}_1 \Delta w_2 - \overline{w}_2 \Delta w_1}{2\overline{w}_1 \sqrt{\overline{w^2}_1}} \end{array} \right\}.$$

Performing similar operations in the y-direction gives

$$\lambda_{1,2,3}^G = \frac{\overline{w}_3}{\overline{w}_1} - \sqrt{\overline{w^2}_1}, \quad \frac{\overline{w}_3}{\overline{w}_1}, \quad \frac{\overline{w}_3}{\overline{w}_1} + \sqrt{\overline{w^2}_1}$$

with

$$\underline{e}_{1,2,3}^G = \left\{ \left(\begin{array}{c} \overline{w}_1 \\ \overline{w}_2 \\ \overline{w}_3 - \overline{w}_1 \sqrt{\overline{w^2}_1} \end{array} \right), \left(\begin{array}{c} 0 \\ \overline{w}_1 \\ 0 \end{array} \right), \left(\begin{array}{c} \overline{w}_1 \\ \overline{w}_2 \\ \overline{w}_3 + \overline{w}_1 \sqrt{\overline{w^2}_1} \end{array} \right) \right\}$$

and

$$\left\{ \begin{array}{c} \alpha_1^G \\ \alpha_2^G \\ \alpha_3^G \end{array} \right\} = \left\{ \begin{array}{c} \Delta w_1 - \frac{\overline{w}_1 \Delta w_3 - \overline{w}_3 \Delta w_1}{2\overline{w}_1 \sqrt{\overline{w^2}_1}} \\ \frac{\overline{w}_1 \Delta w_2 - \overline{w}_2 \Delta w_1}{\overline{w}_1} \\ \Delta w_1 + \frac{\overline{w}_1 \Delta w_3 - \overline{w}_3 \Delta w_1}{2\overline{w}_1 \sqrt{\overline{w^2}_1}} \end{array} \right\}.$$

2.3 Body-Fitted or Cartesian Grids ?

When Roe's scheme is used in two-dimensions for non-Cartesian geometries there are two possibilities for extending the scheme for use in these situations. A body-fitted grid can be used, see Glaister [9] for example. This is certainly the most aesthetically pleasing way of tackling the problem. The main advantage is that it is also efficient in the sense that fewer cells can be used to cover the whole domain. In implementing the method in this way we need to calculate fluxes normal to the cell boundaries, labelled $\underline{D}$ and $\underline{E}$ in Fig. 1. These have a very

similar form to the fluxes already dealt with. (If we label u to be the normal velocity component and v to be the tangential velocity component then all cases are covered by the formulae given for the x-direction previously). Problems with this method are that the domains that can be tackled are limited in complexity, because of the need to generate a quadrilateral mesh to fit it, the 'second order' schemes are limited to formal first order accuracy because of the non-uniformity of the grid, and the grids resulting from a mesh generation routine that creates the mesh according to the geometry of the boundary may not be particularly good for representing the solution in that domain.

(We have also found great difficulty in programming this method. Whilst there may be a bug in the code causing the problems, it does not seem to be very robust and only works for the problems in the next section because the grid actually only varies slightly from being cartesian.)

The other alternative is to use a cartesian grid even though the geometry is non-Cartesian. Obvious advantages are in grid generation and the simplification of the algorithm. Accuracy also formally improves, away from boundaries, as the mesh can be made uniform. On the other hand efficiency decreases since, generally speaking, a greater number of computational cells is needed. However, by the use of overlapping meshes (Priestley [11, 12]), the resolution and efficiency can be greatly improved. More recent advances using this approach by Quirk [14] and Falle & Giddings [7] mean now that it is debatable that whether, for a given accuracy, the body-fitted approach is still more effi-

cient. It should be noted that for efficient programming these approaches can use a quadtree data structure and hence benefit from one of the newer programming languages such as Fortran 90 or C.

The main problem with Cartesian meshes is the modelling of curved, or at least non-aligned, boundaries. There are two approaches to this. There is the staircase method, fig. 2, where the curved boundary is modelled by horizontal and vertical sections, see [7] for example. This looks crude but can be surprisingly effective, especially when combined with the refinement procedures mentioned above. A second method is to model the boundary with discontinuous piecewise linears. Although this also looks a little odd, replacing a smooth boundary by a discontinuous one, it is obviously a better approximation than the staircase. Each sweep now sees that the boundary is not aligned with the cartesian mesh. Also linear shaped boundaries can be approximated exactly, which is an important improvement over the staircase method.

3 Test Problems and Results for the 2-D Shallow Water Equations

The first of the two test problems suggested by ENEL has been tackled in this section. This is a dambreak problem due to Bellos et al. [2, 3, 4]. This consists of an inclined channel 21 metres long and 1.4 metres wide at its widest. There is a constriction in the channel that reduces the width to $0.6m$ at a point $8.5m$ along

the channel. (The coordinates of the channel are measured from -8.5m to 12.5m so that the throat is at 0.0m). A dam is situated at the throat with depths of water h_0 and h_1 upstream and downstream. Precise details of the channel can be found in [2, 3]. The paper [2] is concerned primarily with the collection of experimental data for this problem whilst [3] concentrates on the authors' numerical solution to the same problem. The existence of detailed experimental data makes this a very useful test problem for validating computer models.

In the following we shall take the value of Manning's constant, n, to be 0.012. The acceleration due to gravity will be taken as $9.8ms^{-2}$ and the slope across the channel, β_y, will be assumed to be zero.

The first test problem is taken from Bellos et al. [3]. The slope, β_x, in this case is 0.002. The two depths are $30cm$ and $0cm$ respectively. This means that we are essentially dealing with a dry bed problem. Roe's scheme cannot, always, deal with zero depths as it is particularly sensitive to negative values of depths because of the square roots that need to be taken. These negative depths can be caused by minute oscillations, bearing in mind that we are not guaranteed perfect monotonicity for non-linear equations, or even rounding errors. Hence we shall work with a so called 'damp' bed. The depth of water, where it should be zero, is taken to be a small positive number. In these tests we used a value of depth of 10^{-6} as the smallest permissible. Smaller values have been used but whether these would be as robust is unknown. The solution seems to be unaffected by precisely how large the tolerance is at this scale. We have used tolerances a thousand

times larger and a thousand times smaller and can see no difference in the results.

The results are plotted as four hydrographs at various points along the channel. Fixed time-stepping has been used for all these cases. It should be noted though that considerable savings could be made by using a time-step that responded to the maximum CFL number, as this steadily reduces throughout the computation.

The first solutions are generated on a 40x10 body-fitted mesh, fig. 4. In fig. 5 we see the results of the first order method with a time-step of 0.02. In fig. 6 a temporal refinement is performed and the code is run with a time-step of 0.01. Figure 7 is the same as fig. 6 but now run with the second order scheme using the minmod limiter, equation (2.11). Figure 8 is the same situation as fig. 6 except that it is now run on an 80x20 grid.

Figure 9 shows the result for the same parameters as fig. 5 but with the source terms now upwinded as discussed previously. This is due to the fact that Glaister [9] and Priestley [13] have noticed significant improvements in the solution as a result on occasions. When upwinding of the source terms gives a better solution is unknown. Here it seems to make no difference to the solution obtained.

As can be seen, most of these results are virtually identical. All correspond exceedingly well to the results in [3]. The use of the second order

scheme does 'sharpen up' the profiles visibly although the actual differences in depths with the first order method are very small.

For the cartesian grid approach we have used a 40×40 grid. This gives a slightly more accurate representation at the throat than the body-fitted mesh. Points that fall outside the domain don't involve us in any work and can be ignored. However, we are faced with a great, and unrequired, increase in resolution at the two ends of the domain. We cannot do anything about this in the current code but use of the refinement procedures described in [11, 12] would obviously be a great advantage. In figure 10 we see the first order scheme run with a time-step of $\Delta t = 0.02$ and in fig. 11 we see the results arising from the use of the minmod limiter with a time-step of $\Delta t = 0.01$. In both cases the source terms were evaluated pointwise and the boundary was approximated by the staircase method. Again we see excellent agreement with the experimental results, [3], and only slight differences between the first and second order schemes.

As a second test case we take a problem computed in Bellos et al. [2]. This is the same as the previous case but with a bed-slope of 0.004. We try just two versions of the scheme. The body-fitted grid, fig. 12, and on the cartesian grid, fig. 13. Both are run using the minmod limiter. Again we see excellent agreement with experiment.

4 Roe's Scheme for the 2-D Euler Equations

The 2-D Euler equations, in cartesian co-ordinates are given by

$$\begin{pmatrix} \rho \\ \rho u \\ \rho v \\ e \end{pmatrix}_t + \begin{pmatrix} \rho u \\ \rho u^2 + p \\ \rho uv \\ u(e+p) \end{pmatrix}_x + \begin{pmatrix} \rho v \\ \rho uv \\ \rho v^2 + p \\ v(e+p) \end{pmatrix}_y = \begin{pmatrix} 0 \\ 0 \\ 0 \\ 0 \end{pmatrix}, \tag{4.14}$$

where ρ is the fluid density, u & v are the fluid velocities. The momenta, ρu & ρv, are usually replaced by new variables m & n. The static pressure is denoted by p and e is the total energy and is related to the other variables by an equation of state, which for a perfect gas is

$$e = \frac{p}{(\gamma - 1)} + \frac{1}{2}\rho u^2,$$

although other gas laws are possible. The constant γ is the ratio of specific heats and takes a value of 1.4 for our calculations. Two other variables that are needed in deriving Roe's scheme for the Euler equations are the total enthalpy, $h = (e + p)/\rho$ and the sound speed, $a = (\gamma p/\rho)^{\frac{1}{2}}$. Here we will not specifically derive the scheme as the algebra is entirely analagous to that given in section 2 and formulae for the wave strengths etc. are all well known and given elsewhere, see Roe [15], for example.

In axially symmetric co-ordinates the Euler equations become,

$$(4.15)\qquad \begin{pmatrix} \rho \\ \rho u \\ \rho v \\ e \end{pmatrix}_t + \frac{1}{R}\begin{pmatrix} R\rho u \\ R\rho u^2 \\ R\rho uv \\ Ru(e+p) \end{pmatrix}_R + \begin{pmatrix} \rho v \\ \rho uv \\ \rho v^2 + p \\ v(e+p) \end{pmatrix}_z = \begin{pmatrix} 0 \\ -p_R \\ 0 \\ 0 \end{pmatrix}.$$

Glaister [9] applied Roe's scheme to these equations by defining new variables, $\mathcal{R} = R\rho, U = Ru, P = Rp$ etc. The only term that is not accounted for by Roe's scheme is then put on the right-hand side, $\underline{b} = (0, p, 0, 0)^T$. Alternatively, we can expand the R derivatives in (4.15) and we are left with equations identical to those in (4.14), if we identify the R direction with the y co-ordinate and the z direction with the x co-ordinate in those equations, but now with the source term given by $\underline{b} = (1/R)(-\rho u, -\rho u^2, -\rho uv, -u(e+p))^T$.

The advantage of Glaister's approach is that there are less terms left to be accounted for as source terms, but the disadvantage is that we are required to use transformed variables. The advantage of the second approach is that one code can be used for 2-D cartesian geometries and 2-D axially symmetric flows just by the addition of an extra source term. We shall adopt the second approach here. Glaister also found advantage in upwinding his source term as it was readily identifiable with the direction of R increasing. Our source terms, now more numerous, have no such obvious linking with either of the co-ordinate directions and so we evaluate the source terms pointwise with no obvious ill-effect showing in the results.

The test problem is that used by Cooke & Fansler [5] for which there exists experimental data, see references in [5]. It consists of a blast wave exiting from a shock tube. The dimensions of the problem are all given in [5] and are also illustrated in figure (14). We plot time-histories of the overpressure, the pressure above or below atmospheric pressure, at 8 points. The first 6 of these points lie on an arc of a circle of radius 1.5 radiating from the centre of the opening of the circular shock tube, position (1,0) in our axially symmetric co-ordinates. The points are then placed at angles $\psi = 0^o, 30^o, 60^o, 90^0, 120^0$ and 130^o. The seventh point lies on the face of the shock tube at co-ordinates (1,0.74) and the eighth point lies on the upper surface of the shock tube at position (0.54,1), see figure (14). The initial conditions are taken to be atmospheric outside of the shock tube, that is the velocities are zero, $\rho = 1.22kg/m^3$ and $p = 100kPa$. Inside the tube the radial velocity, v, is still taken as zero but the other components are $u = 332m/s, \rho = 2.78kg/m^3$ and $p = 342kPa$.

The calculations were, except where otherwise stated, performed on a mesh of 120×60 points. Time-steps were chosen to give maximum CFL numbers of just under 1/2.

Figures (15–18) give contour plots of the pressure at times 200, 500, 1000 and $1500\mu s$ for a solution calculated by the first order scheme. Figure (19) shows the time-histories at the selected points for the first order method. Comparing with the exact solution and calculations given in Cooke & Fansler [5] the contour plots look acceptable but the time-histories are rather disappointing.

Although the general shapes and positions are all correct they are clearly too smoothed and the peak values are equally clearly not at the correct values. In figures (20–23) and (24) we give the same results but now calculated with a second order scheme (Van Leer's limiter). We recall that in the dambreak problem the improvement obtained by using a second order scheme was somewhat less than dramatic. The contour plots are much the same as for the first order case. The real differences are in the time-histories, fig. (24). Here there has been a very real sharpening of some of the profiles, compare the feature at position 2 at around $1000\mu s$. Not only have the features been sharpened up but peaks have taken on values much closer to the expected physical values; see the first peak at position 1, for example, where the peak value has increased by 10%.

In some respects these calculations are better than those of [5] but in one place we do seem to have got the wrong answer. At position 1 the transition to negative overpressure appears to occur noticeably too soon, an error of over 10%. This occurs for both methods. To see what might be causing this we tried running the second order scheme on a finer mesh. This produces figure (25). We note only a marginal improvement in most of the figures but the position of this feature has definitely moved in the right direction. (To be fair to the method here we ought to note that other methods also fail to get this feature in the correct place. This may be due to the numerical interpolation used to calculate the value at that point as suggested in Cooke & Fansler [5]). The other thing to check is the effect of the far field boundary conditions. These have been taken to be supersonic boundary conditions, which is a very dubious assumption

for much of the boundary. Hence we ran the second order scheme again on a domain of twice the size on the 240x120 mesh, that is, at the same resolution as the original problem. These results are shown in figure (26) and are, to all intents and purposes, identical to those on the smaller region.

5 Conclusions

In this report we have investigated the use of Roe's scheme for two problems involving systems of conservation laws in two dimensions; namely, the shallow water equations and the Euler equations of gas flow. Having developed the method for both of these systems of equations in one and two dimensions, two test problems were tackled for which there exists experimental data. A dam-break problem was investigated using the shallow water equations, and a blast wave exiting from a shock tube was solved with the Euler equations.

One novel feature of the work tried here was the comparison of body-fitted grids with cartesian grids. Although body-fitted grids were more efficient than cartesian grids for the "valley" of figure (4), the situation is often reversed. If body-fitted grids need extra points for resolution in one region it is difficult to vary the grid and it is necessary to work with this grid density throughout the whole domain. The cartesian grids offer not only a substantial simplification of the algorithm but also, though not attempted here, the possibility of variable resolution leading ultimately, for larger problems, to greater efficiency.

Source terms arose in both problems, and in the past these have sometimes been found to give problems with TVD schemes. Here we compared the effect of pointwise evaluation and upwinding of the source terms. No difference was detected and we concluded that the character of the source terms in these test problems was not such as to provide the conditions for the difficulties experienced elsewhere.

All the results showed a very good agreement with the experimental results obtained by other authors. The first order algorithm showed itself to be adequate in some situations but the second order flux limited scheme showed itself to be clearly superior for the harder blast wave problem.

Finally we conclude that this feasibility study has shown Roe's scheme to be capable of providing results in excellent agreement with experimental data, at least for these two application areas. The potential of the method, in particular the use of nested cartesian grids, has not been fully explored here but looks very promising. This, together with more realistic problems, could be the subject of further investigation.

6 Acknowledgements

The author wishes to acknowledge the cooperation of Dr. P. Molinaro of ENEL-CRIS in suggesting the problems solved in this report and for his general help. The work was sponsored by ENEL-CRIS under a contract with the Institute

for Computational Fluid Dynamics in the Department of Mathematics at the University of Reading, U.K..

References

[1] Baines, M.J., *"Numerical Algorithms for the Non-Linear Scalar Wave Equation."* University of Reading Numerical Analysis Report 1/83, 1983.

[2] Bellos, C.V., Soulis, J.V. & Sakkas, J.G., *"Experimental Investigation of Two-Dimensional Dam-Break Induced Flows"*. J. of Hydraulic Res., **30**, pp.47-63, 1992.

[3] Bellos, C.V., Soulis, J.V. & Sakkas, J.G., *"Computation of Two-Dimensional Dam-Break Induced Flows"*. Adv. Water Resources, **14**, pp. 31-41, 1991.

[4] Bellos, C.V., Soulis, J.V. & Sakkas, J.G., *"Computing 2-D Unsteady Open-Channel Flow by Finite-Volume Method"*. Proc. VII Int. Conf. on Comp. Meth. in Water Resources, Vol. 1, Eds. M.A. Celia, L.A. Ferrand, C.A. Brebbia, W.G. Gray and G.F. Pinder, pp. 357-362, 1988.

[5] Cooke, C.H. & Fansler, K.S., *"Comparison with Experiment for TVD Calculations of Blast Waves from a Shock Tube."* Int. J. for Numer. Meth. in Fluids **9**, pp. 9-22, 1989.

[6] Deconinck, H., Hirsch, Ch. & Peuteman, J., *"Characteristic Decomposition Methods for the Multidimensional Euler Equations."* Lecture Notes in

Physics **264**, pp. 216-221, Springer, 1986.

[7] Falle, S.A.E.G. & Giddings, J.R., *"Body Capturing Using Adaptive Cartesian Grids.'* In Numerical Methods for Fluid Dynamics IV, Proc. of the Conf. on Numerical Methods for Fluid Dynamics, University of Reading 1992, Eds. K.W. Morton & M.J. Baines, OUP.

[8] Glaister, P., *"Shock Capturing Schemes for Body-Fitted Meshes."* Int. J. Numer. Meth. Fl. **8**, pp. 1095-1105, 1988.

[9] Glaister, P., *"Flux-Difference Splitting for the Euler Equations with Axial Symmetry."* J. Eng Math. **22**, pp. 107-121, 1988.

[10] Hirsch, C. & Lacor, C., *"Upwind Algorithms based on a Diagonalization of the Multidimensional Euler Equations."* AIAA paper 89-1958, 1989.

[11] Priestley, A., *"Roe's Scheme, Euler Equations, Cartesian Grids, Non-Cartesian Geometries, Rigid Walls and all that."* University of Reading Numerical Analysis Report 14/87, 1987.

[12] Priestley, A., *"Roe's Scheme, Euler Equations, Cartesian Grids, Non-Cartesian Geometries, Rigid Walls and there's more."* University of Reading

Numerical Analysis Report 9/88, 1988.

[13] Priestley, A., *"The use of a Characteristic Based Scheme for the 2-D Shallow Water Equations."* Techniques for Horizontal Discretization in Numerical Weather Prediction Models, pp. 157-185, ECMWF Workshop Proceedings, 1987.

[14] Quirk, J.J., *"An Alternative to Unstructured Grids for Computing Flows Around Arbitrarily Complex Two-Dimensional Bodies.'* In Numerical Methods for Fluid Dynamics IV, Proc. of the Conf. on Numerical Methods for Fluid Dynamics, University of Reading 1992, Eds. K.W. Morton & M.J. Baines, OUP.

[15] Roe, P.L., *"Approximate Riemann Solvers, Parameter Vectors, and Difference Schemes."* J. Comp. Phys., **43**, pp. 357-372, 1981.

[16] Roe, P.L., *"Large Scale Computations in Fluid Mechanics."* Lectures in Applied Mathematics, **22**, no. 2, pp. 163-193, 1985.

[17] Roe, P.L., *"Discrete Models for Numerical Analysis of Time-Dependent Multi-Dimensional Gas Dynamics."* J. Comp. Phys, **63**, pp. 458-476, 1986.

[18] Strang, G., *"On the Construction and Comparison of Difference Schemes."* SIAM J. Numer. Anal., **5**, pp. 506-517, 1968.

[19] Sweby, P.K., *"High Resolution Schemes Using Flux Limiters for Hyperbolic Conservation Laws."* SIAM J. Numer. Anal., **21**, pp. 995-1011, 1984.

[20] Sweby, P.K., *"High Resolution TVD Schemes Using Flux Limiters."* Lectures in Applied Mathematics, Vol. 22, Springer, 1985.

[21] Van Leer, B., *"Towards the Ultimate Conservative Difference Scheme II. Monotonicity and Conservation Combined in a Second Order Scheme."* J. Comp. Phys., **14**, pp. 361-371, 1974.

List of Figures

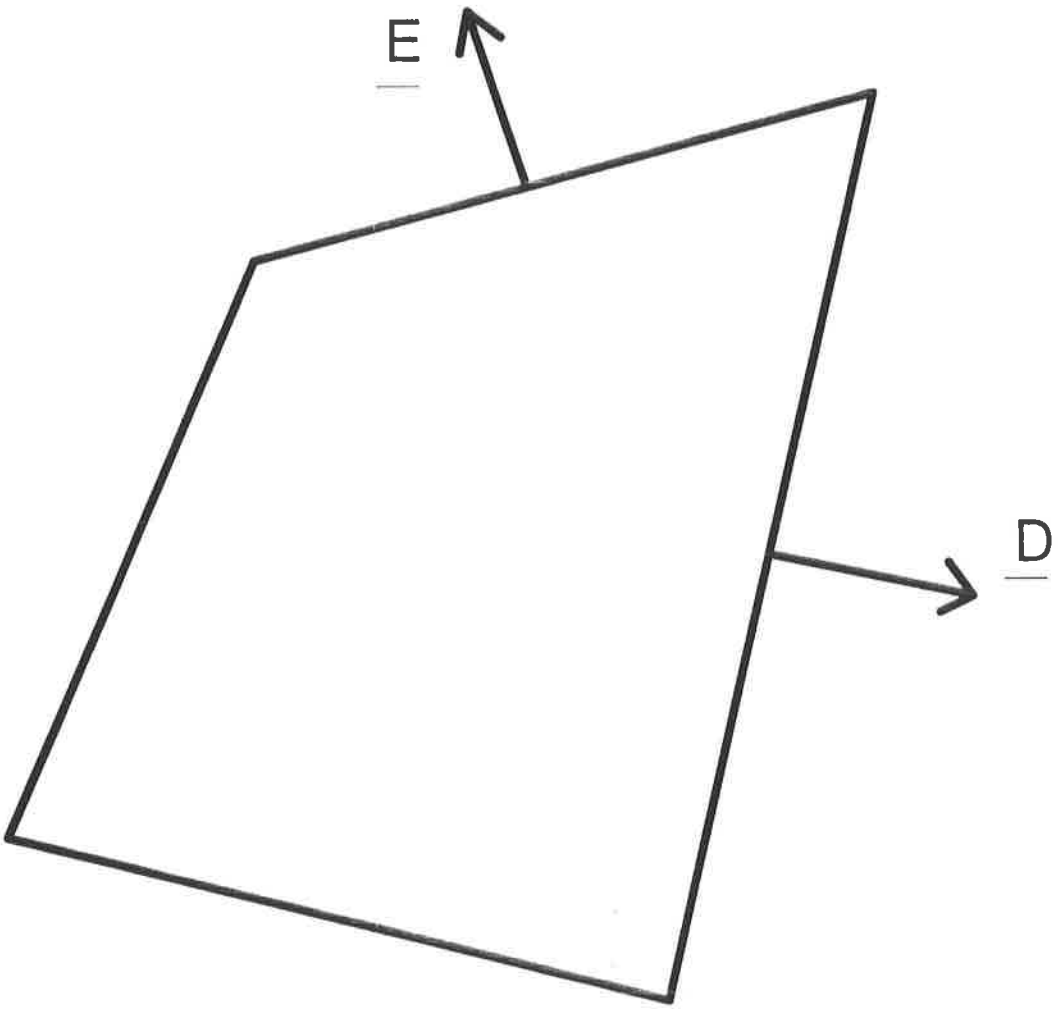

Figure 1: Fluxes used on a body-fitted grid.

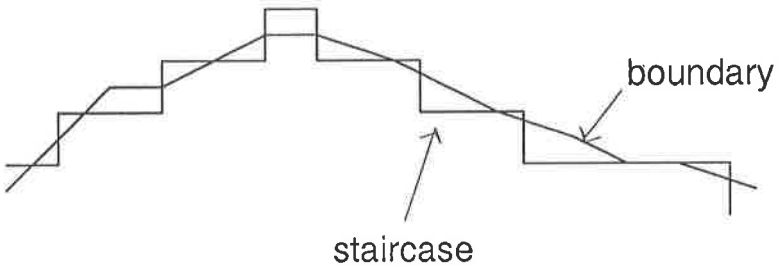

Figure 2: Staircase approach to approximation of boundaries on Cartesian meshes.

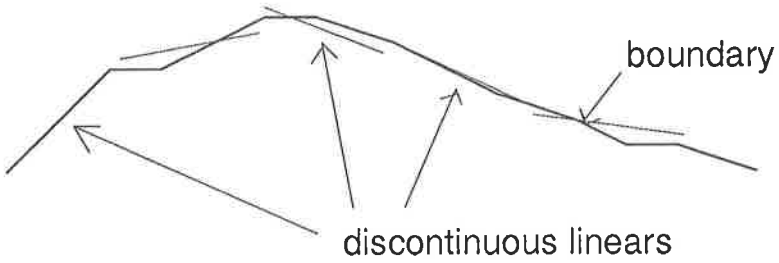

Figure 3: Discontinuous piecewise linear approach to approximation of boundaries on Cartesian meshes.

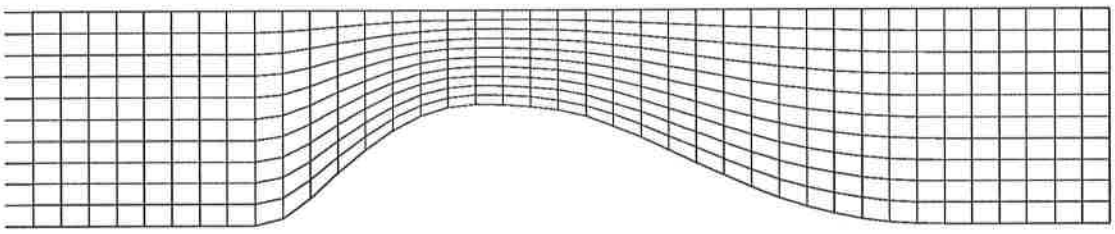

Figure 4: Body fitted grid (40x10) for dam-break problem.

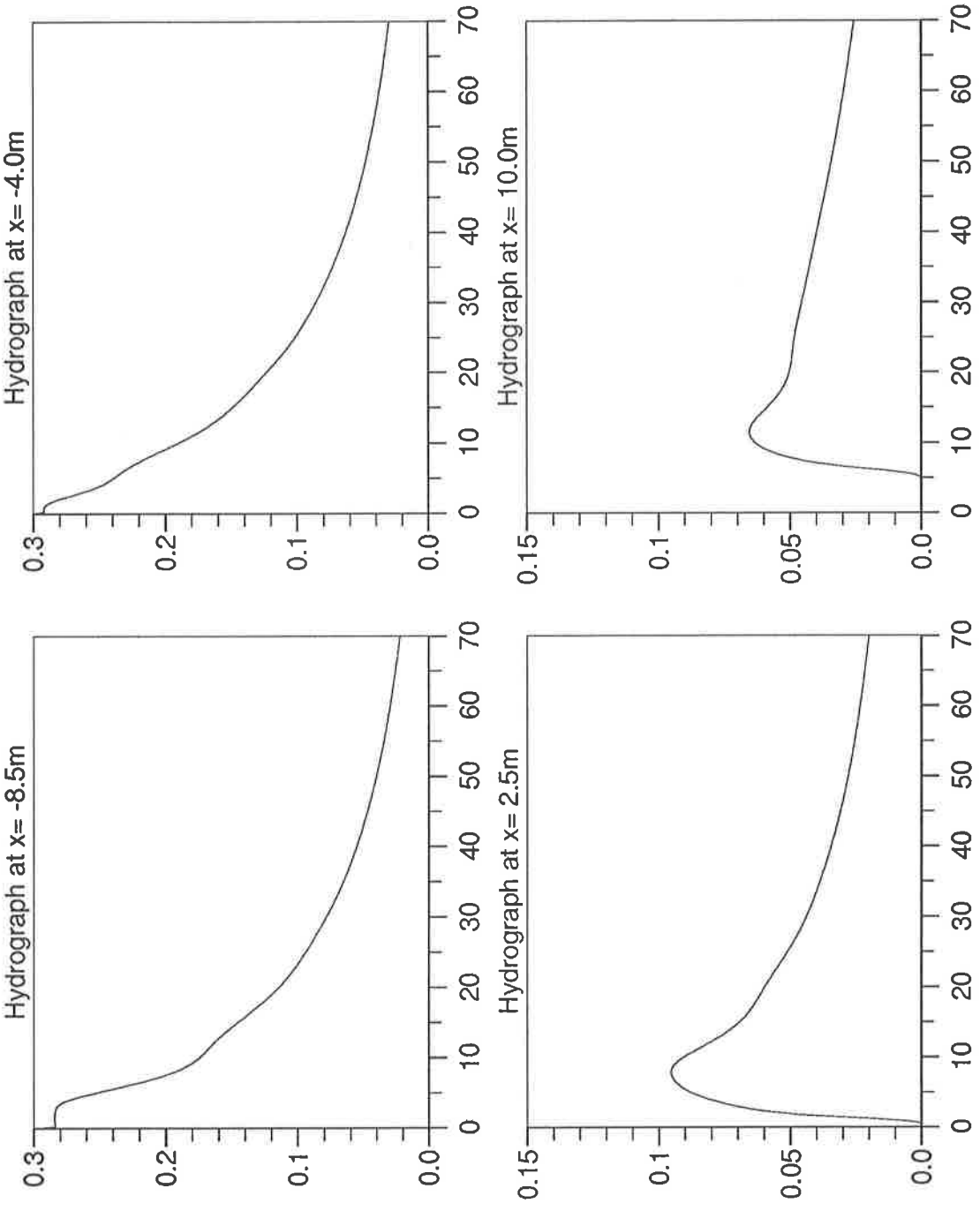

Figure 5: Body fitted grid (40x10), 1^{st} order scheme, $\beta_x = 0.002$, $\Delta t = 0.02$.

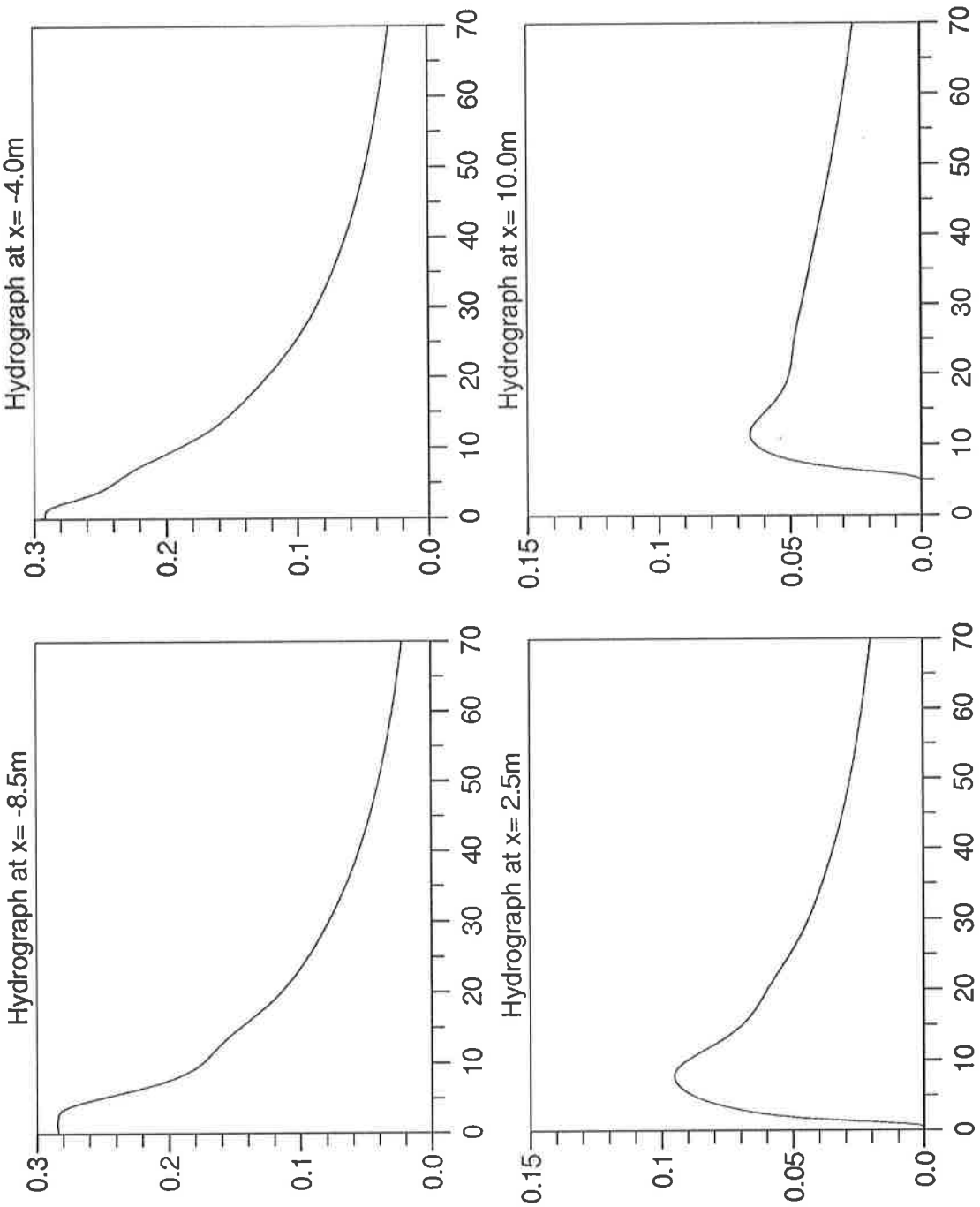

Figure 6: Body fitted grid (40x10), 1^{st} order scheme, $\beta_x = 0.002$, $\Delta t = 0.01$.

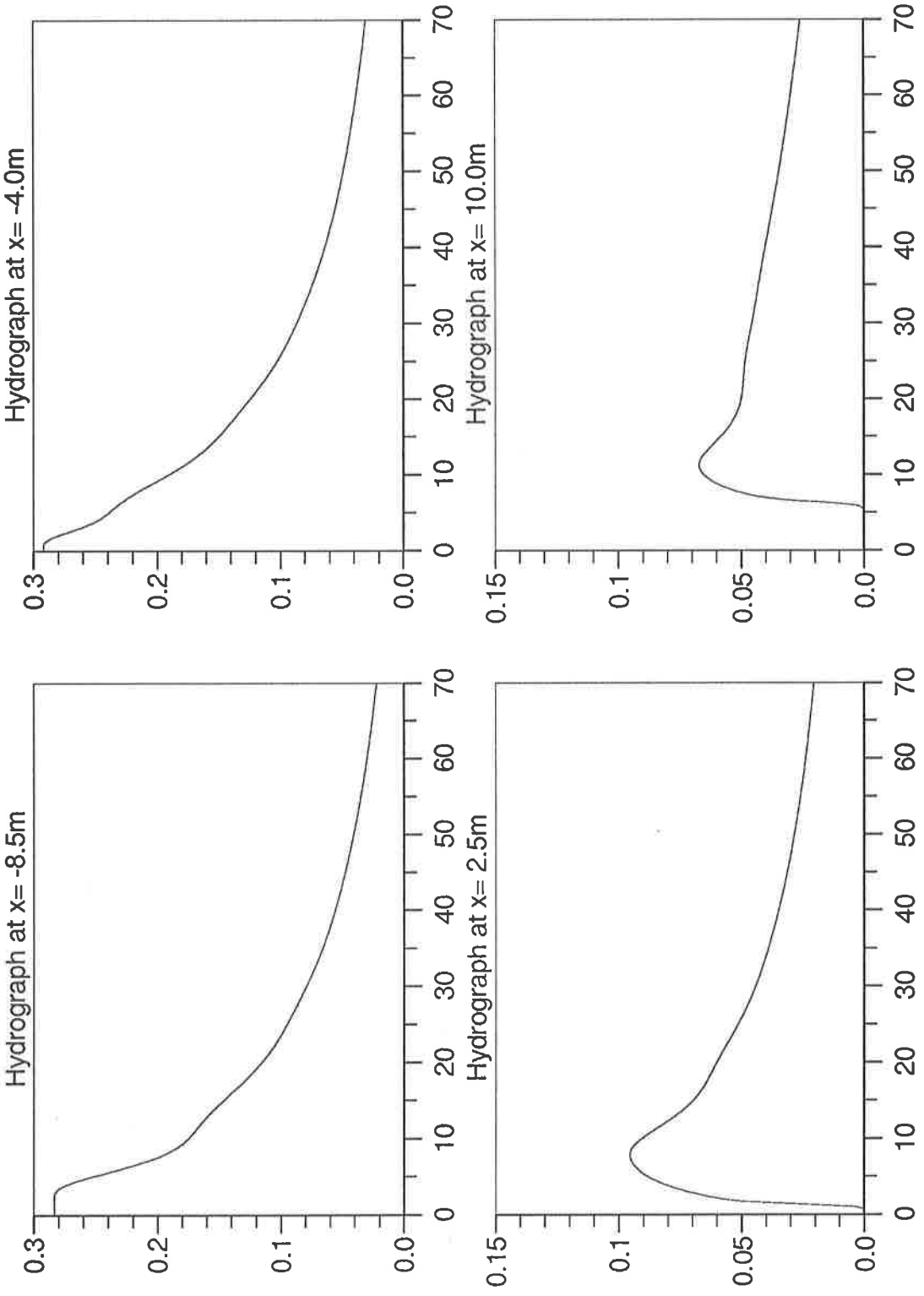

Figure 7: Body fitted grid (40x10), minmod limiter, $\beta_x = 0.002$, $\Delta t = 0.01$.

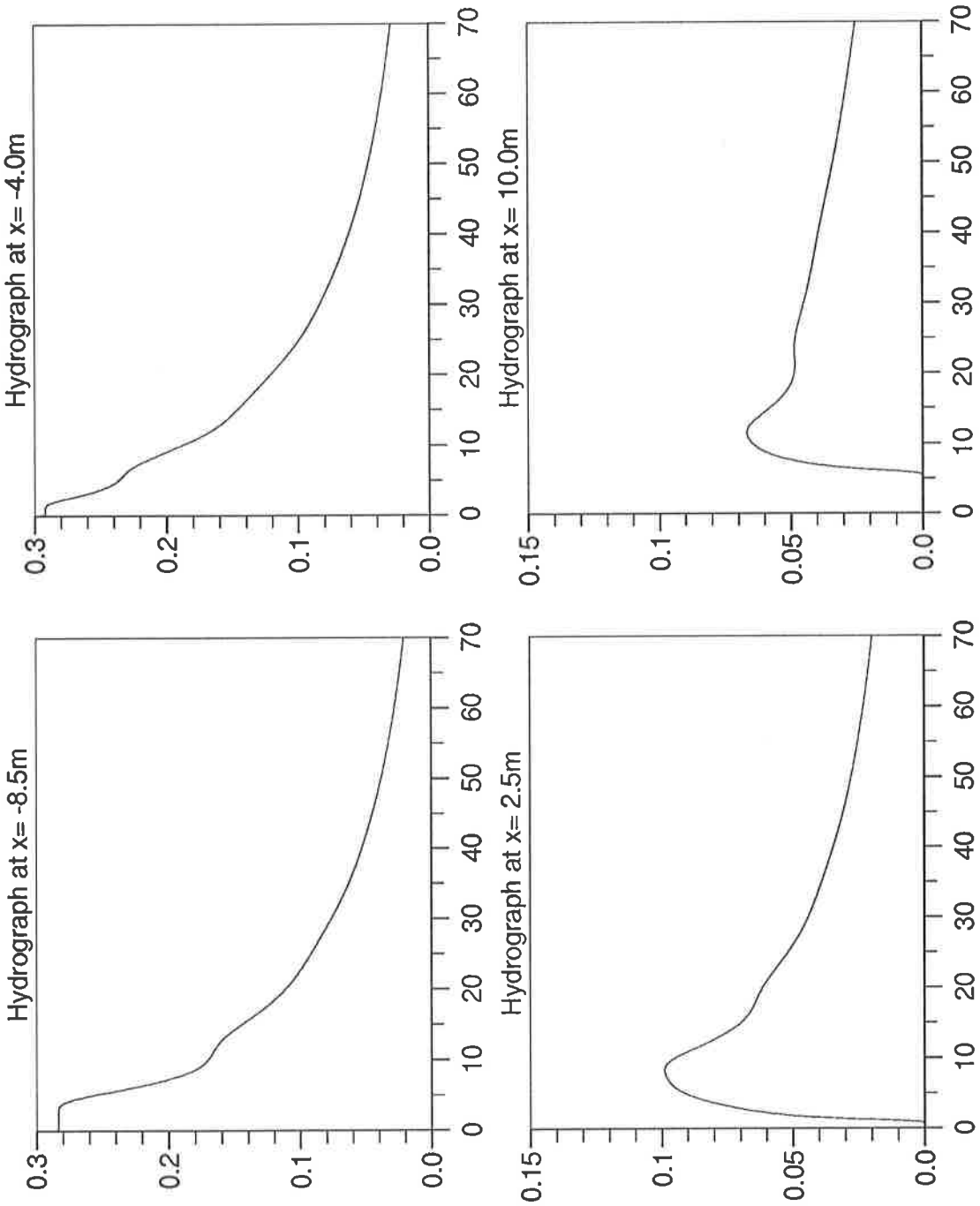

Figure 8: Body fitted grid (80x20), 1^{st} order scheme, $\beta_x = 0.002$, $\Delta t = 0.01$.

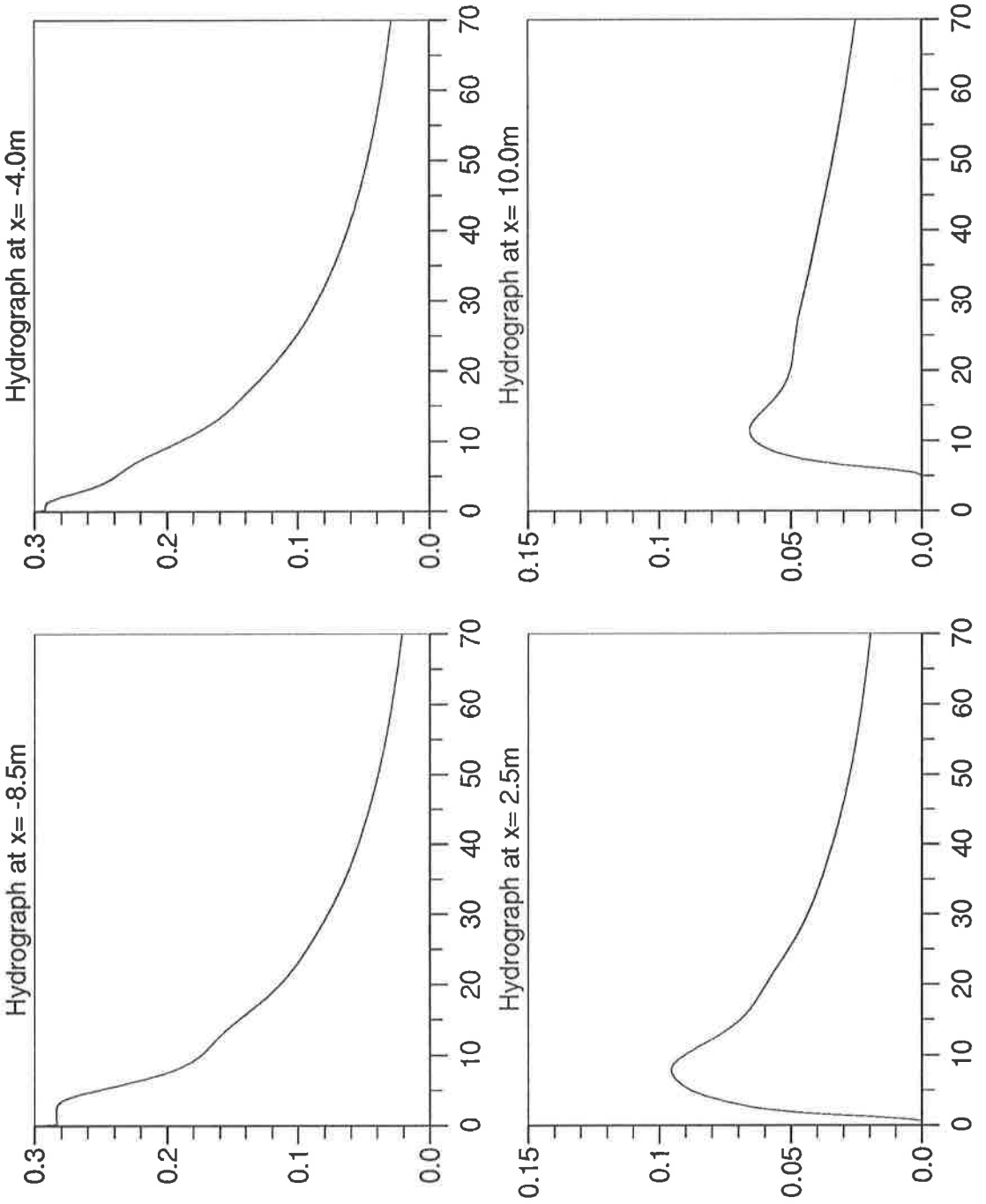

Figure 9: Body fitted grid (40x10), 1^{st} order scheme, $\beta_x = 0.002$, $\Delta t = 0.02$. Upwinded source terms.

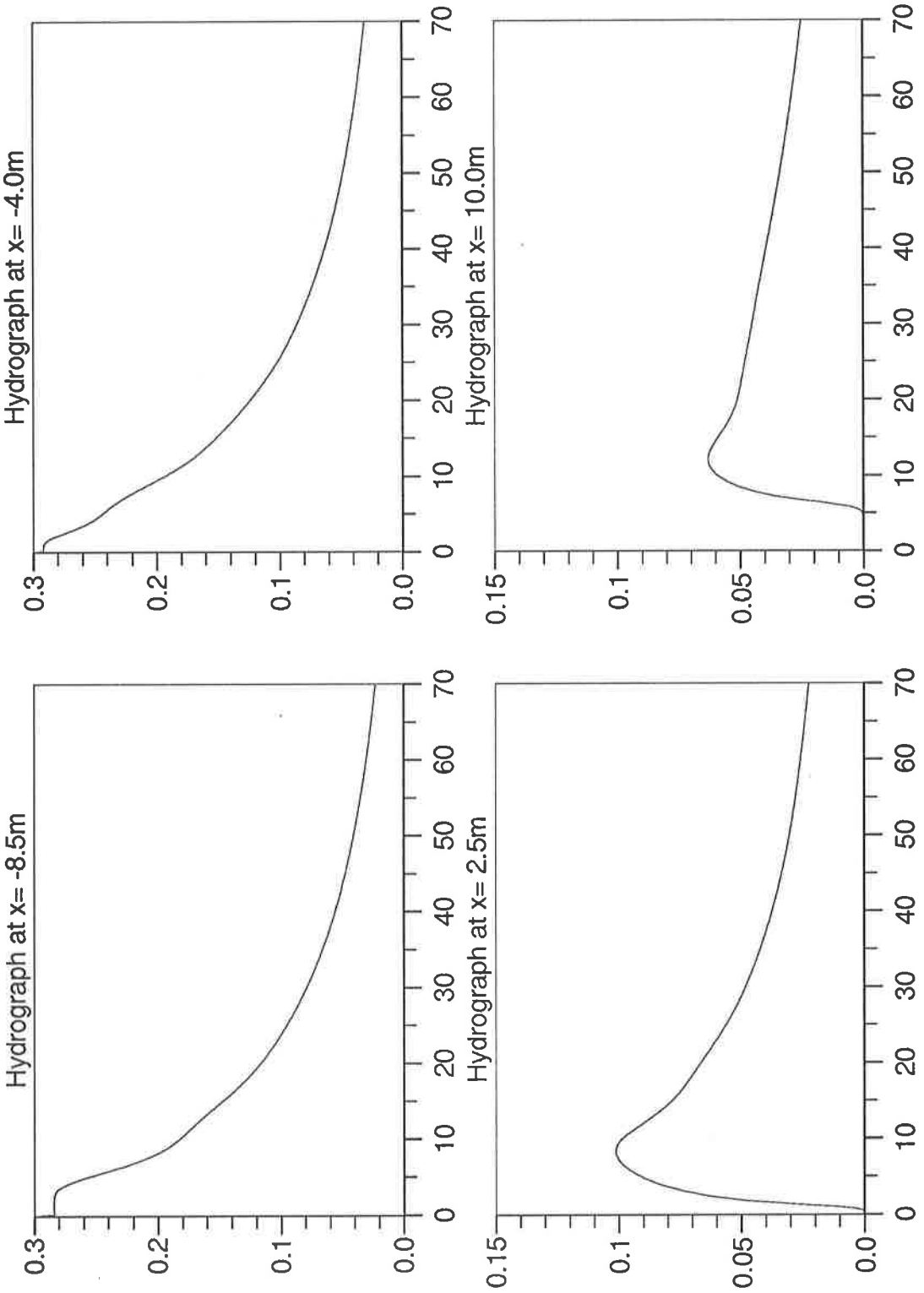

Figure 10: Cartesian grid (40x40), 1^{st} order scheme, $\beta_x = 0.002$, $\Delta t = 0.02$.

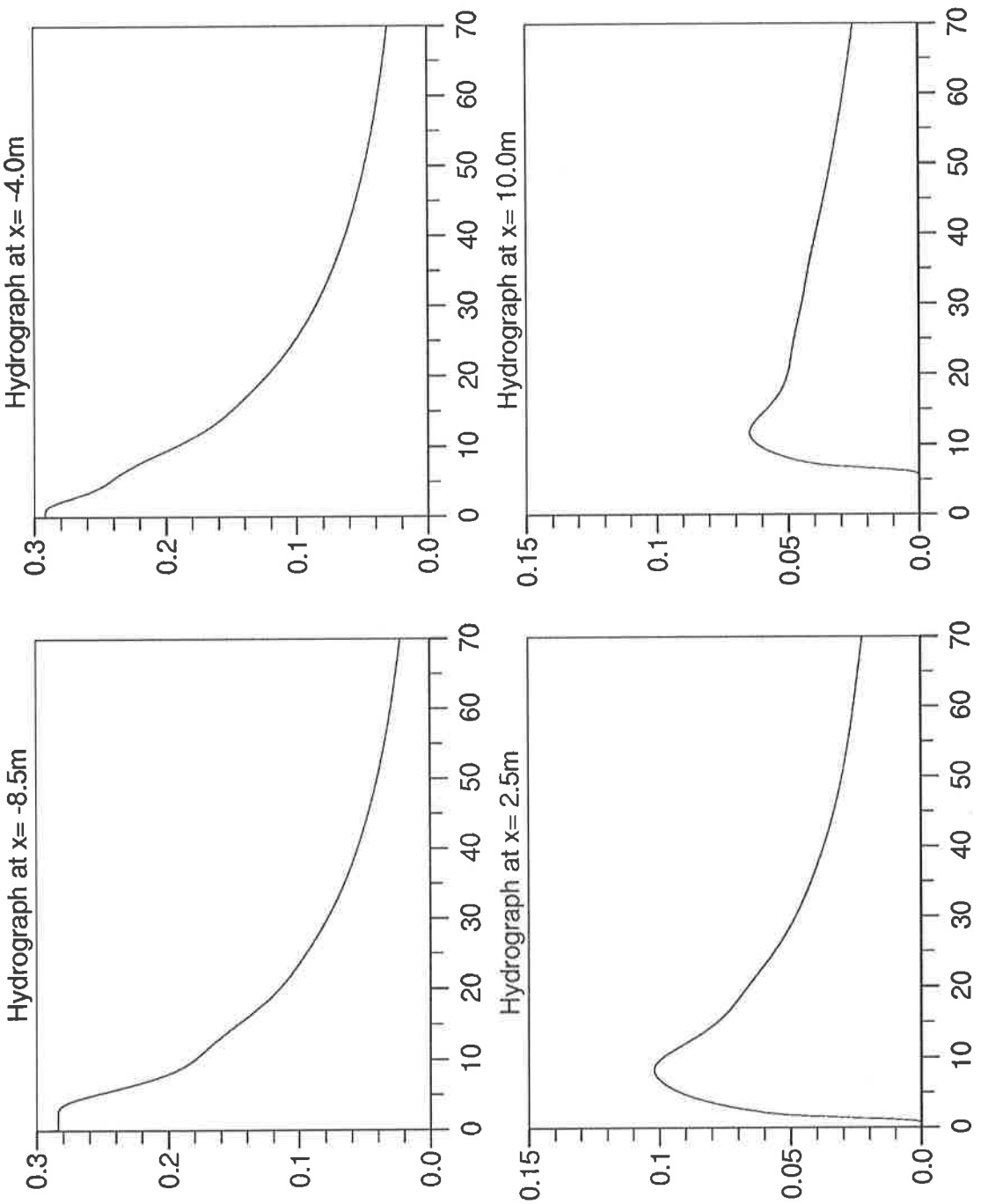

Figure 11: Cartesian grid (40x40), minmod limiter, $\beta_x = 0.002$, $\Delta t = 0.01$.

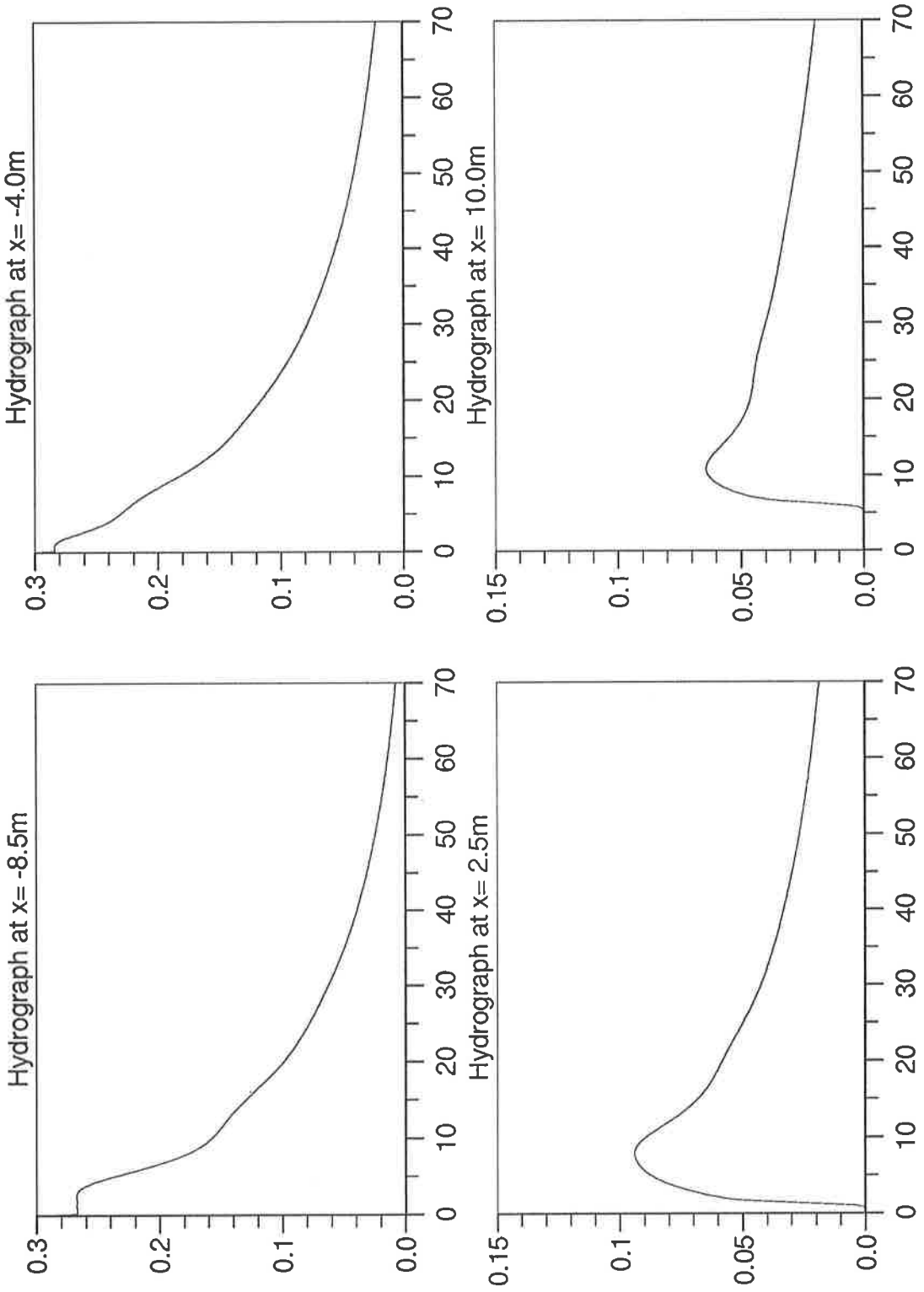

Figure 12: Body-fitted grid (40x10), minmod limiter, $\beta_x = 0.004$, $\Delta t = 0.02$.

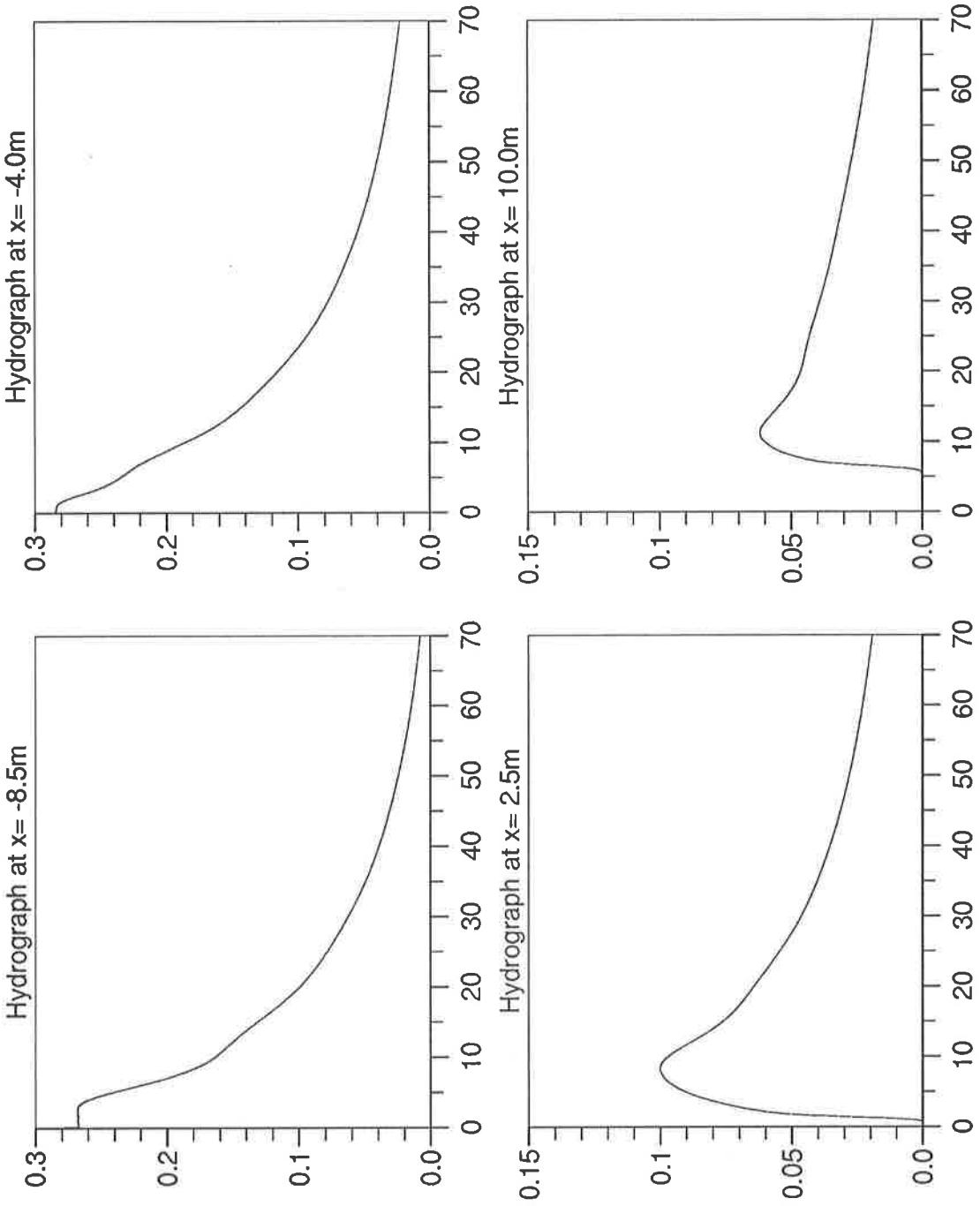

Figure 13: Cartesian grid (40x40), minmod limiter, $\beta_x = 0.004$, $\Delta t = 0.01$.

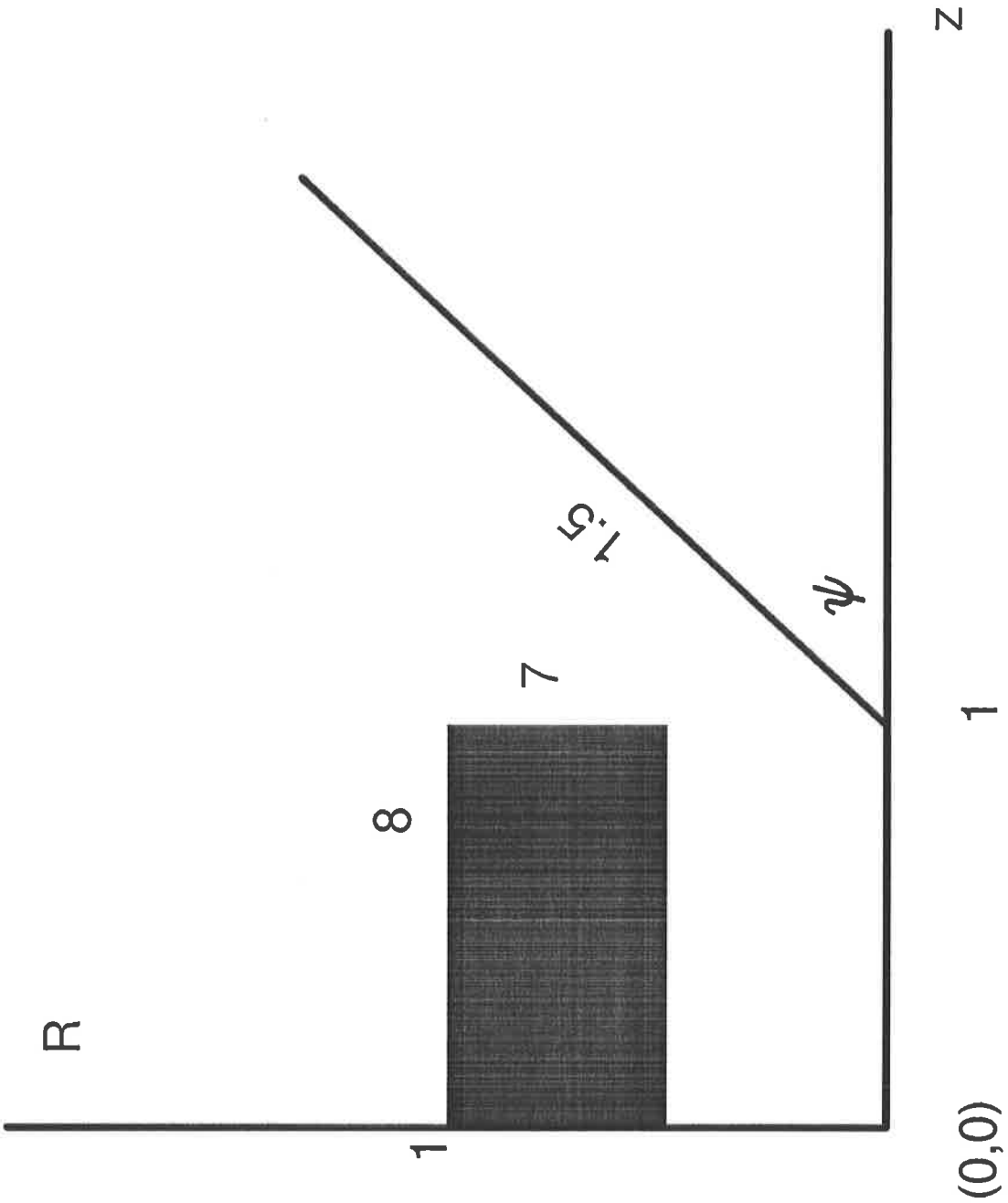

Figure 14: Geometry of the exiting shock wave problem with position of observed points.

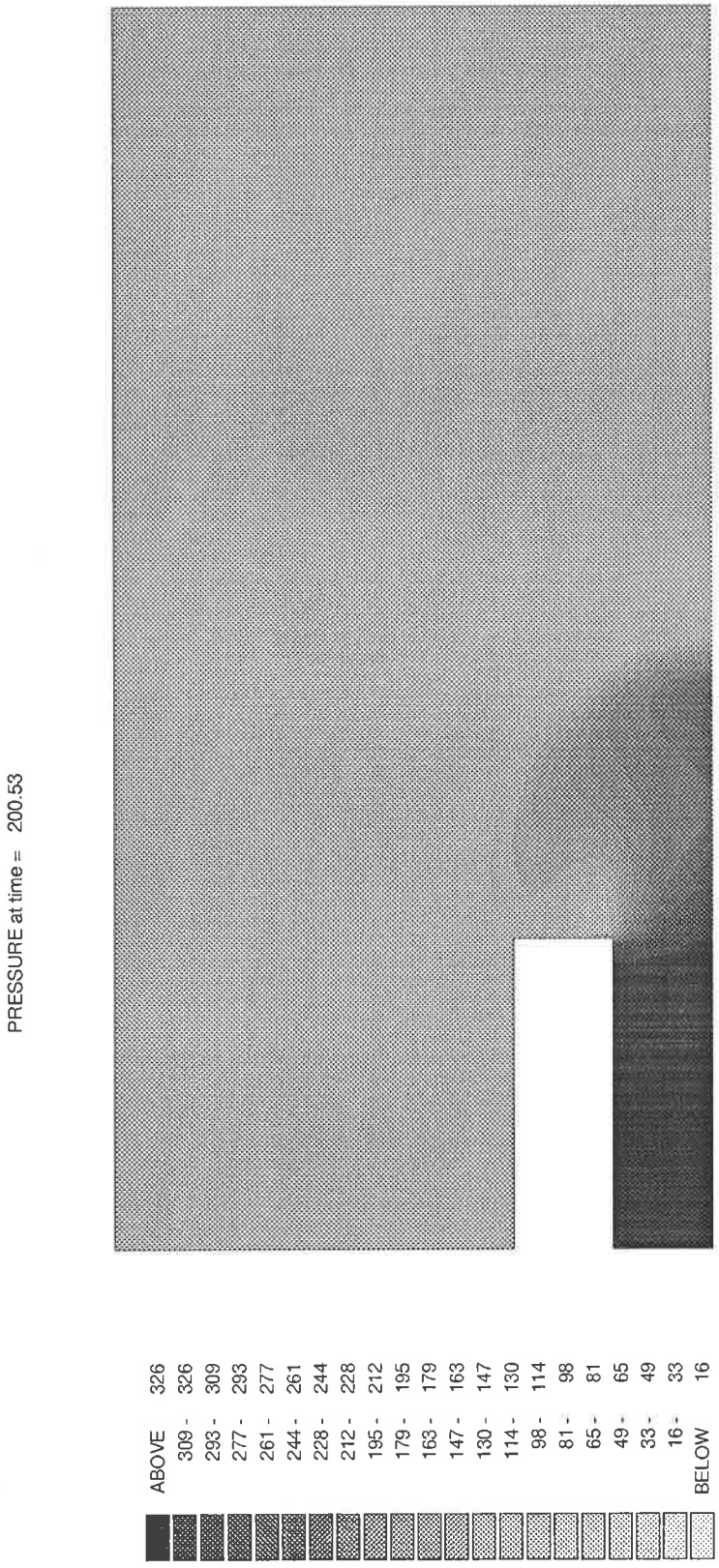

Figure 15: Pressure contours (kPa.) for the flow from a shock tube using a 1^{st} order scheme on a 120x60 grid.

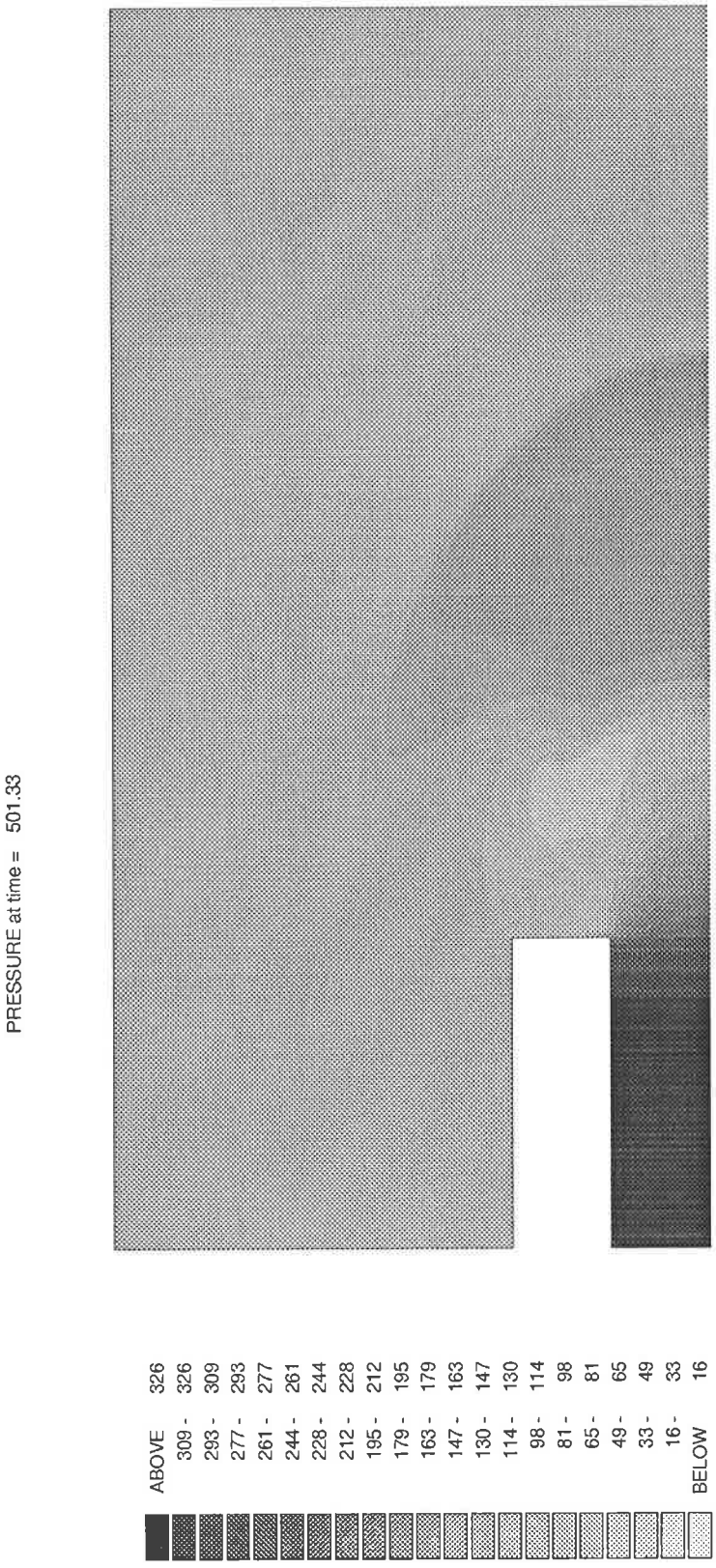

Figure 16: Pressure contours (kPa.) for the flow from a shock tube using a 1^{st} order scheme on a 120x60 grid.

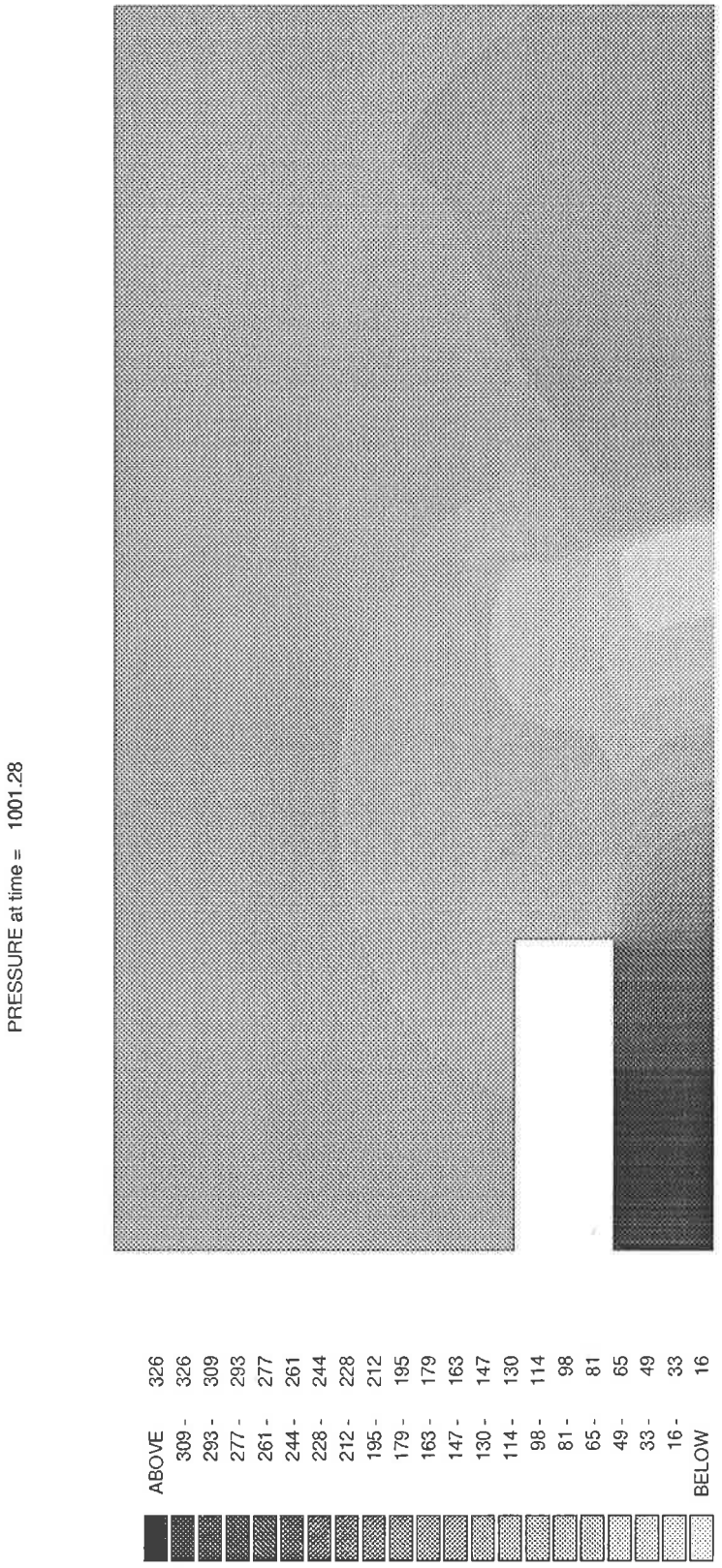

Figure 17: Pressure contours (kPa.) for the flow from a shock tube using a 1^{st} order scheme on a 120x60 grid.

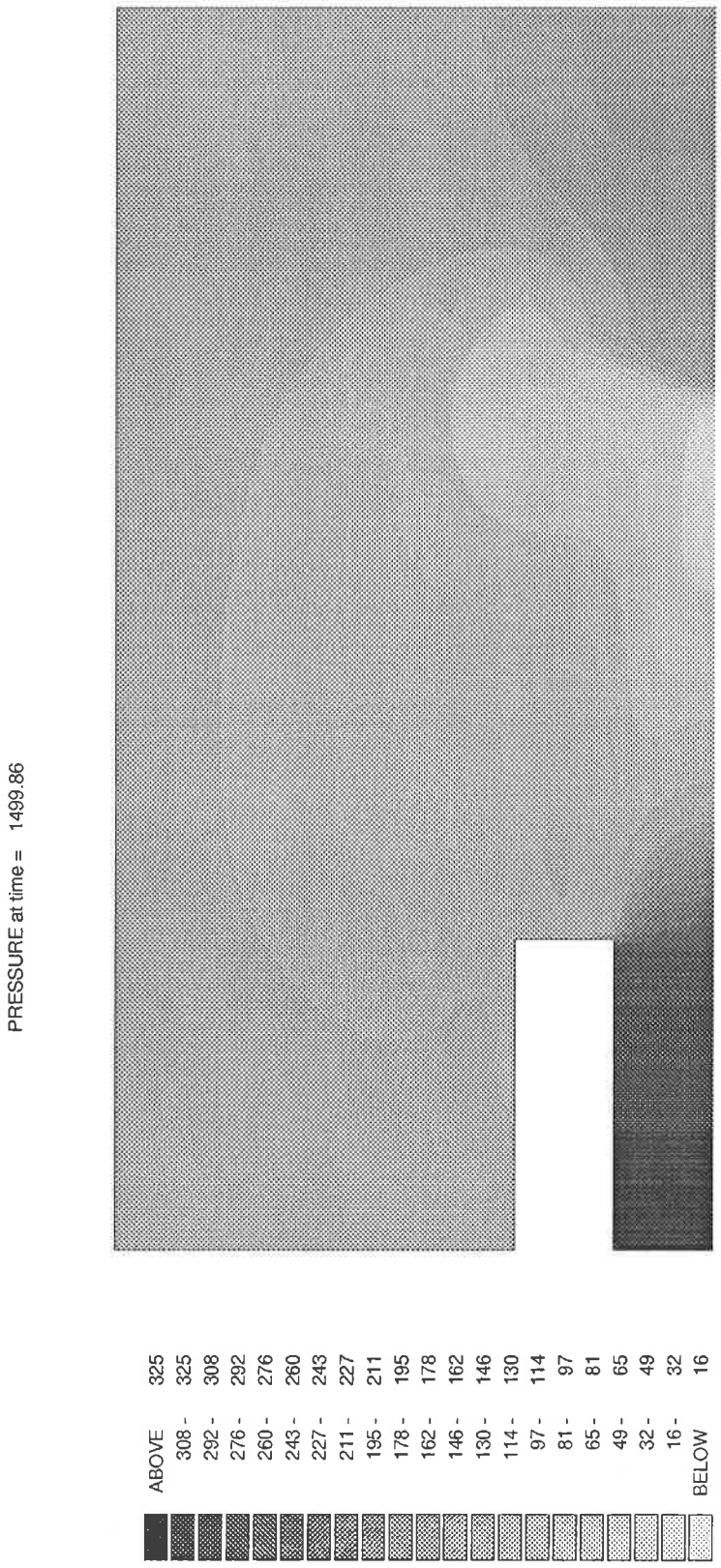

Figure 18: Pressure contours (kPa.) for the flow from a shock tube using a 1^{st} order scheme on a 120x60 grid.

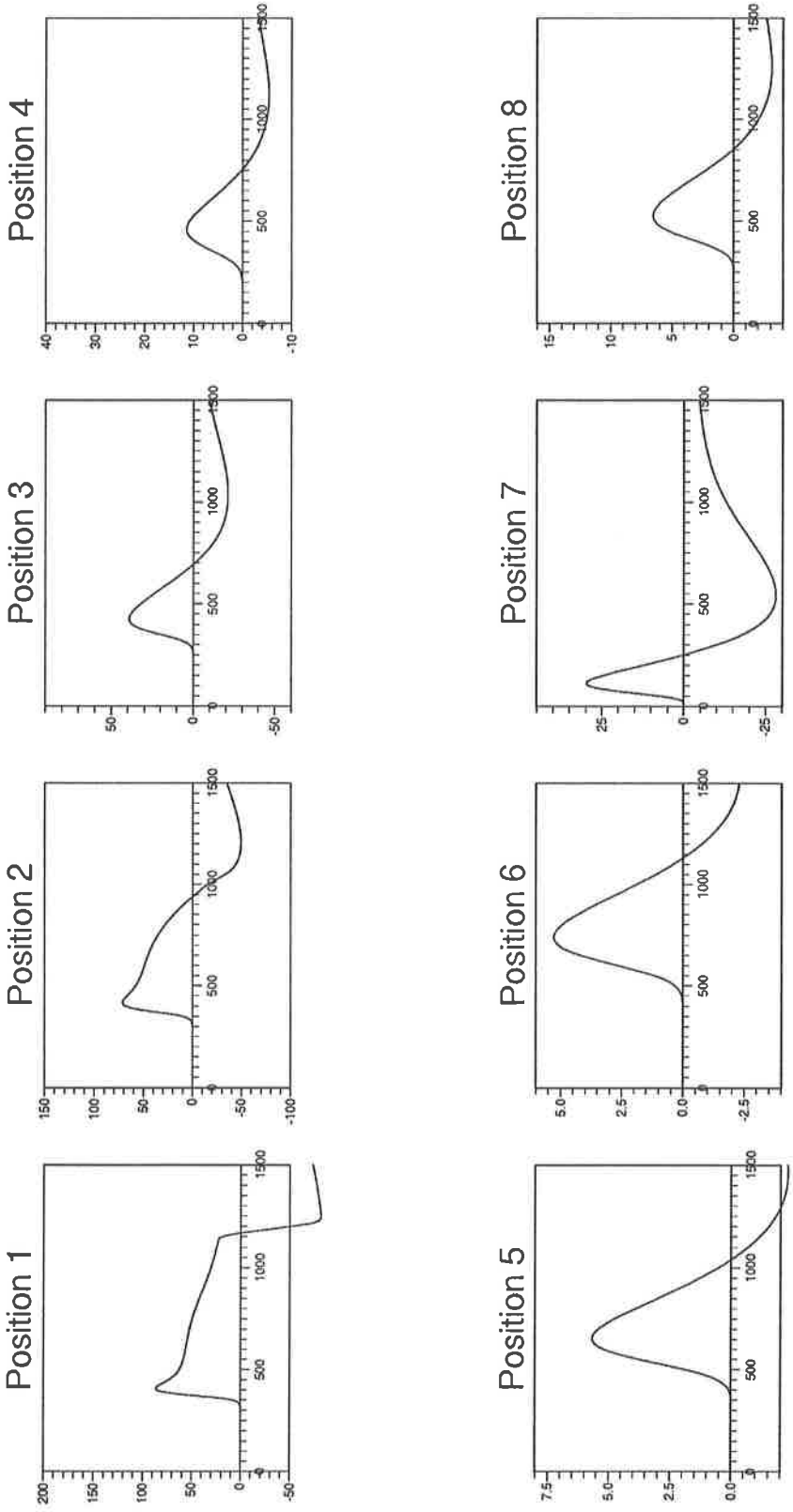

Figure 19: Time histories of overpressure (kPa.) against time (μs) for the flow from a shock tube using a 1^{st} order scheme on a 120x60 grid.

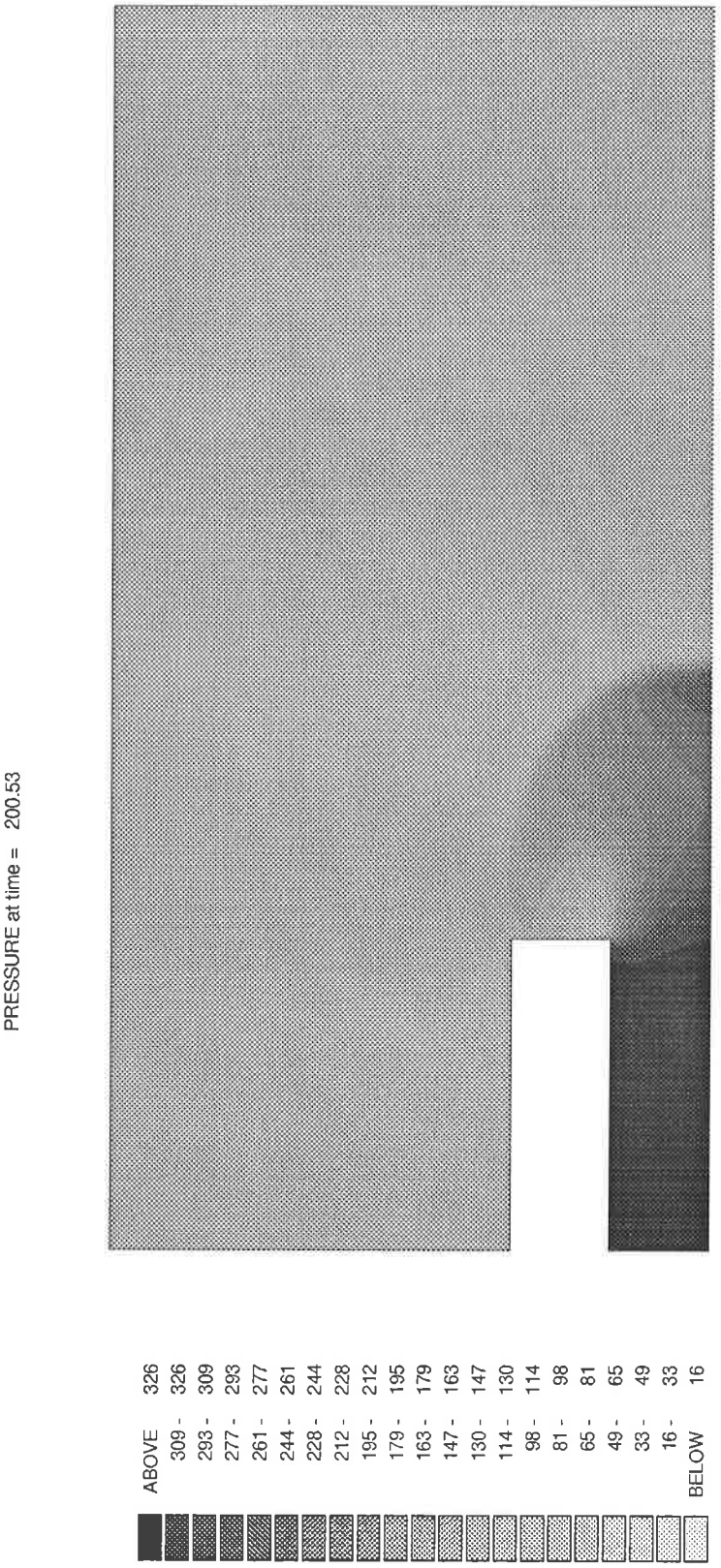

Figure 20: Pressure contours (kPa.) for the flow from a shock tube using Van Leer's limiter on a 120x60 grid.

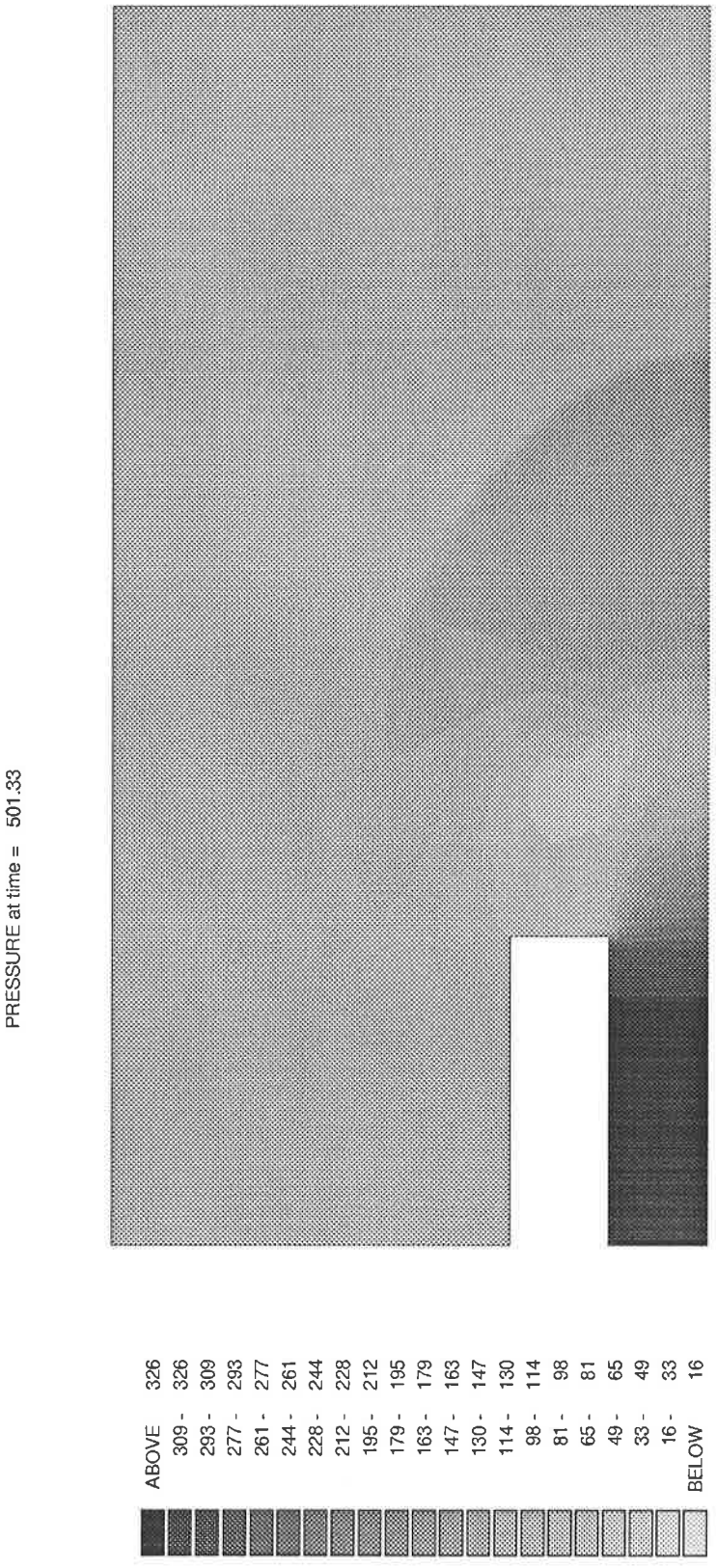

Figure 21: Pressure contours (kPa.) for the flow from a shock tube using Van Leer's limiter on a 120x60 grid.

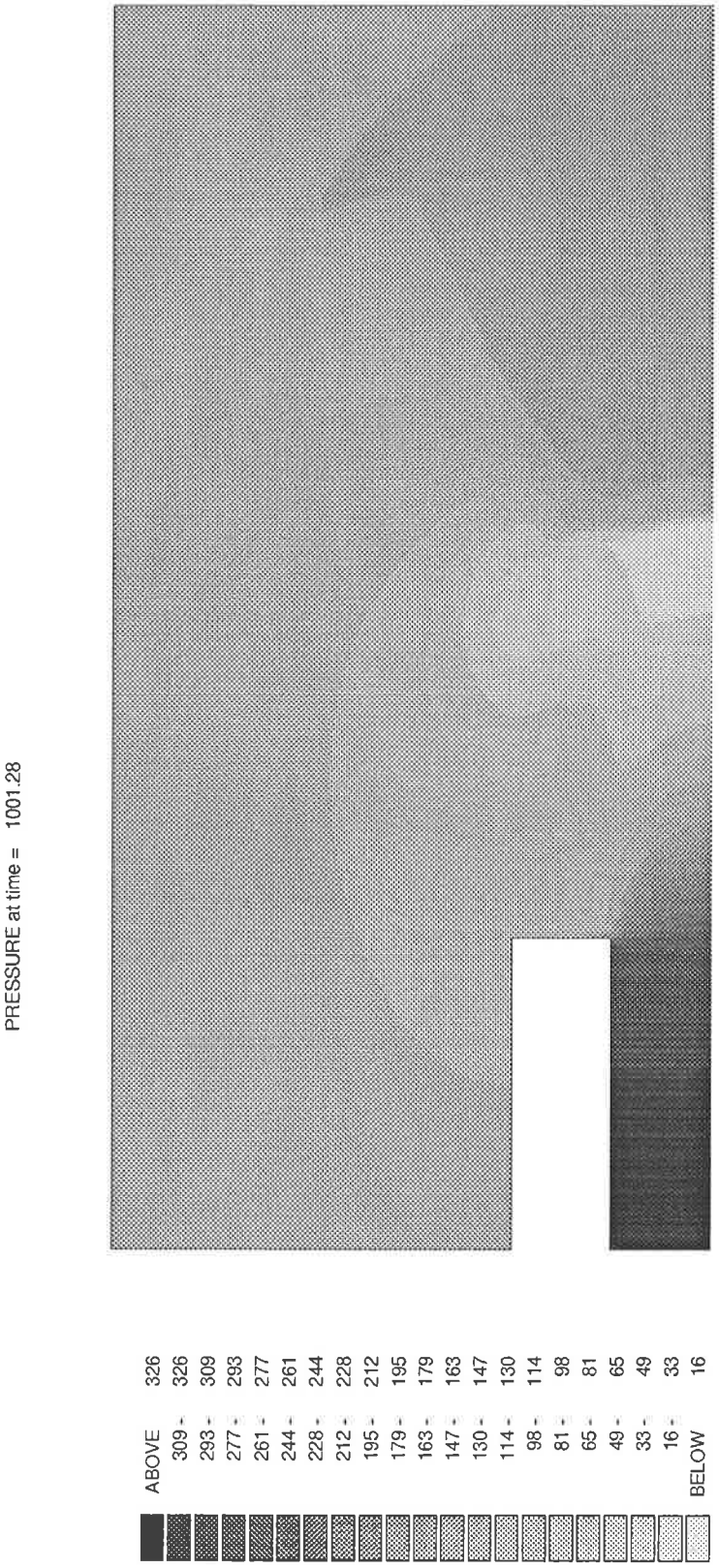

Figure 22: Pressure contours (kPa.) for the flow from a shock tube using Van Leer's limiter on a 120x60 grid.

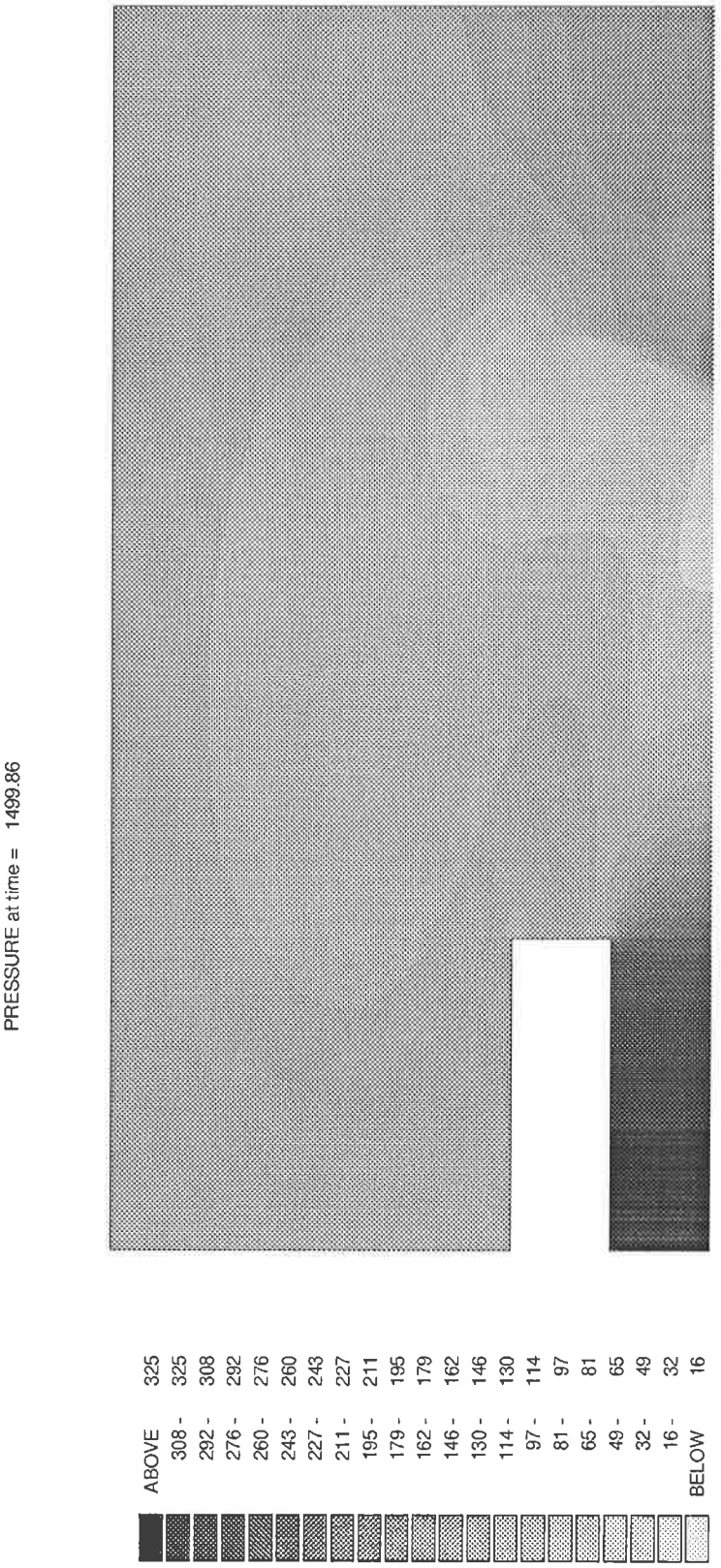

Figure 23: Pressure contours (kPa.) for the flow from a shock tube using Van Leer's limiter on a 120x60 grid.

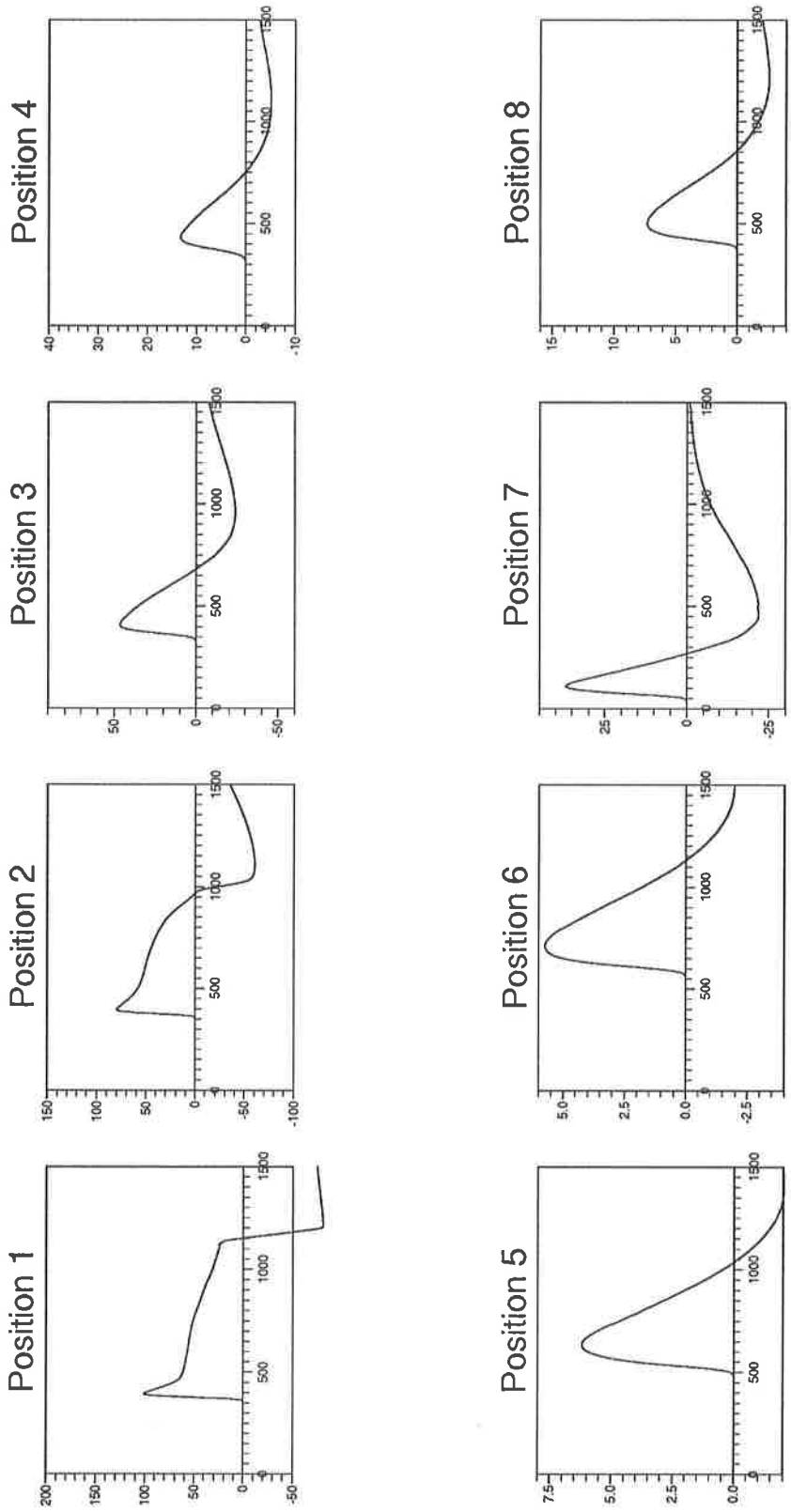

Figure 24: Time histories of overpressure (kPa.) against time (μs) for the flow from a shock tube using Van Leer's limiter on a 120x60 grid.

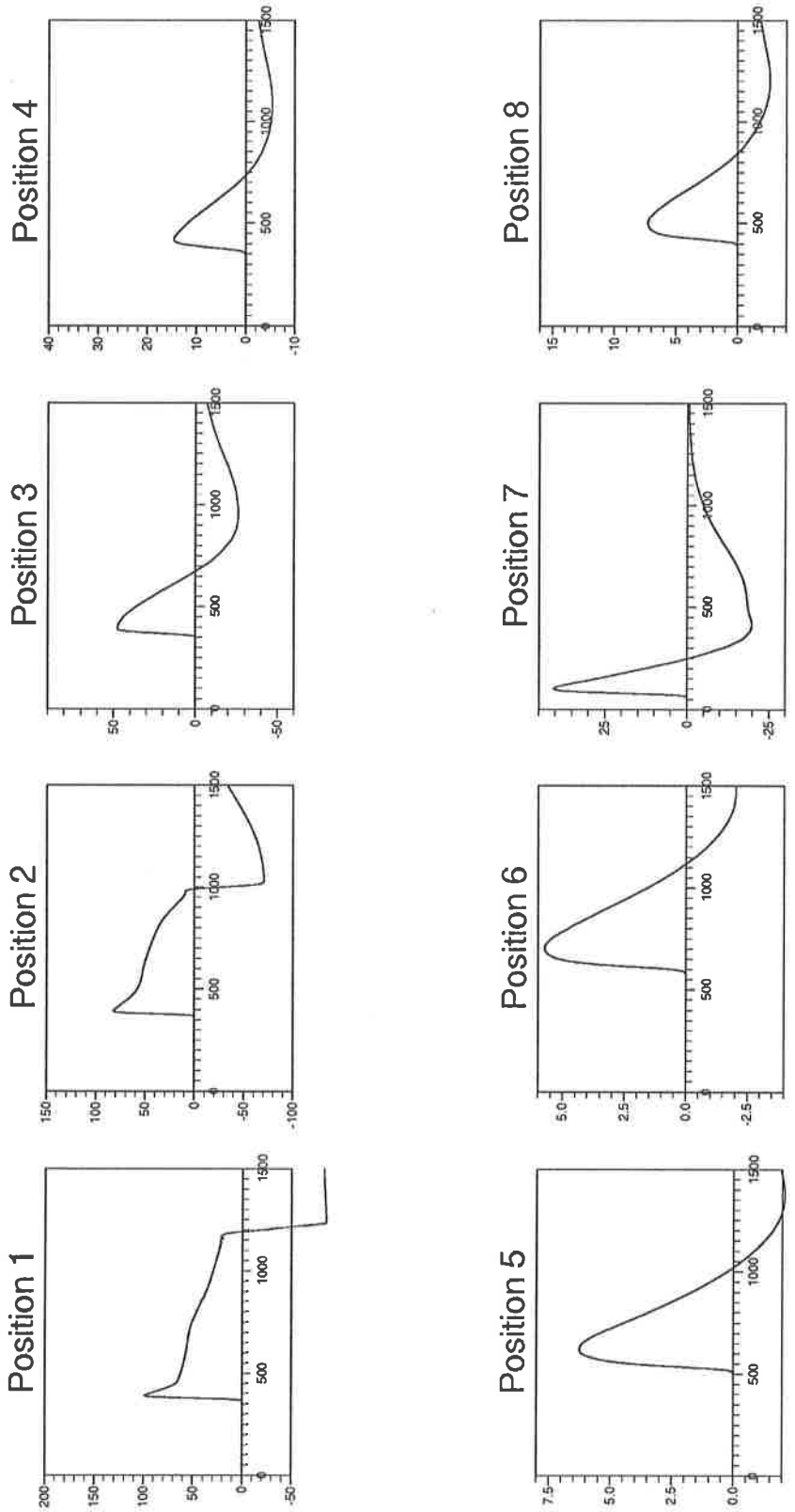

Figure 25: As figure (24) but on a 240x120 grid.

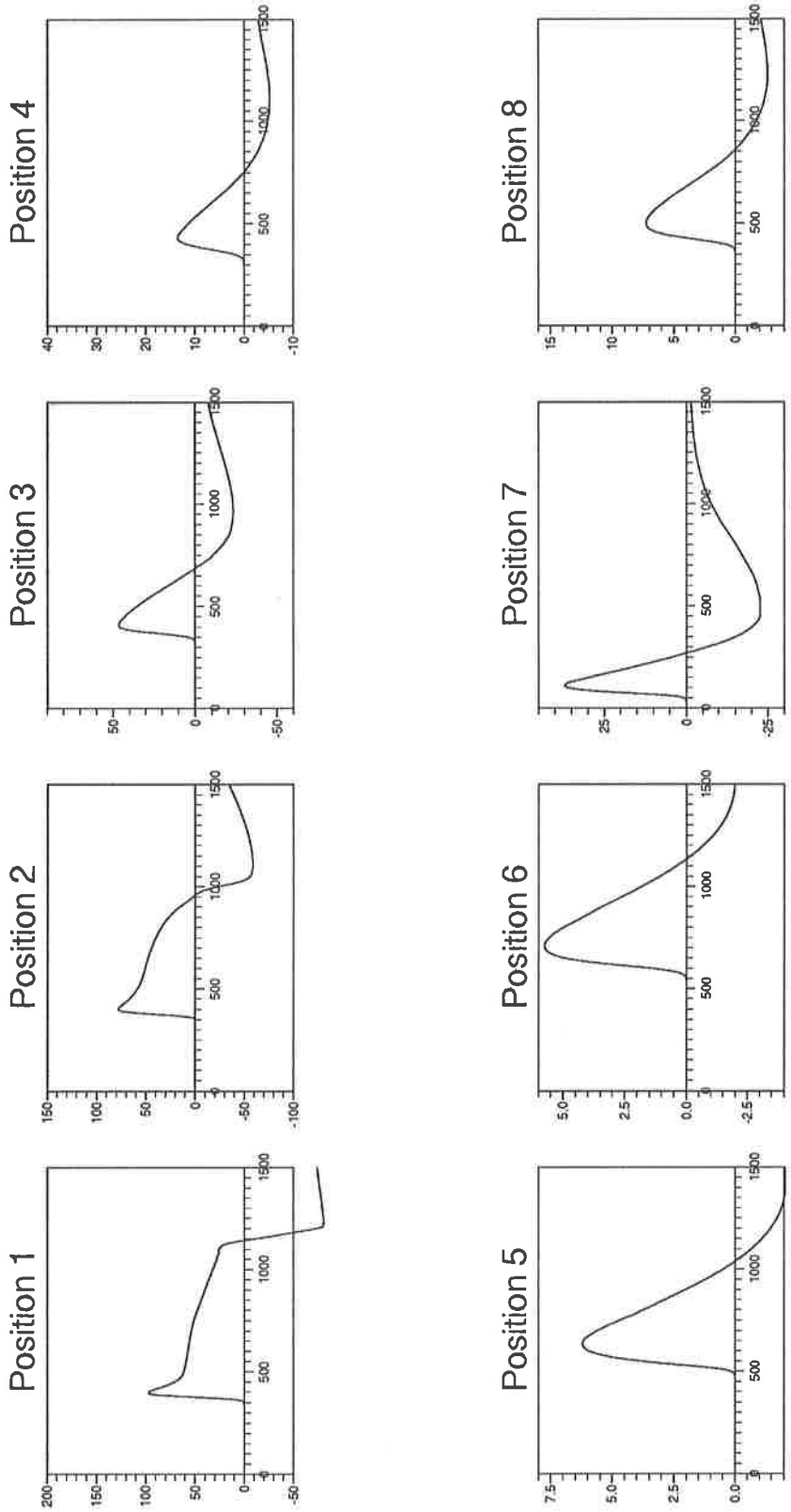

Figure 26: As figure (25) but on a domain of double size.